The versican-hyaluronan complex provides an essential extracellular matrix niche for Flk1^{+} hematoendothelial progenitors

[1] Sumeda Nandadasa, [1] Anna O'Donnell, [2]Ayako Murao, [2]Yu Yamaguchi, [1] Ronald J. Midura, [3]Lorin Olson, and [1,*] Suneel S. Apte

[1] Department of Biomedical Engineering (ND20), Cleveland Clinic Lerner Research Institute, 9500 Euclid Avenue, Cleveland, OH 44195

[2]Human Genetics Program, Sanford Burnham Prebys Medical Discovery Institute, La Jolla, CA 92037

[3]Cardiovascular Biology Research Program, Oklahoma Medical Research Foundation, Oklahoma City, OK 73104

[*]Corresponding author: Suneel S. Apte, MBBS, D.Phil., Department of Biomedical Engineering-ND20, Lerner Research Institute, Cleveland Clinic, 9500 Euclid Avenue, Cleveland, OH 44195, USA. Phone: 216.445.3278; E-mail: aptes@ccf.org

Short title: Versican and hyaluronan in vasculogenesis

Abstract

Little is known about extracellular matrix (ECM) contributions to formation of the earliest cell lineages in the embryo. Here, we show that the proteoglycan versican and glycosaminoglycan hyaluronan are associated with emerging Flk1^{+} hematoendothelial progenitors at gastrulation. The mouse versican mutant *Vcan*^{hdf} lacks yolk sac vasculature, with attenuated yolk sac hematopoiesis. CRISPR/Cas9-mediated *Vcan* inactivation in mouse embryonic stem cells reduced vascular endothelial and hematopoietic differentiation within embryoid bodies, which generated fewer blood colonies, and had an impaired angiogenic response to $VEGF_{165}$. Hyaluronan was severely depleted in *Vcan*^{hdf} embryos, with corresponding upregulation of the hyaluronan-depolymerase TMEM2. Conversely, hyaluronan-deficient mouse embryos also had vasculogenic suppression but with increased versican proteolysis. $VEGF_{165}$ and Indian hedgehog, crucial vasculogenic factors, utilized the versican-hyaluronan matrix, specifically versican chondroitin sulfate chains, for binding. Versican-hyaluronan ECM is thus an obligate requirement for vasculogenesis and primitive hematopoiesis, providing a vasculogenic factor-enriching microniche for Flk1^{+} progenitors from their origin at gastrulation.

KEYWORDS: Proteoglycan; vasculogenesis; angiogenesis; endothelium; hematopoiesis CRISPR-Cas9

Introduction

The first blood vessels in amniotes form *de novo* in the yolk sac prior to initiation of hemodynamic forces, indicating an in situ differentiation driven by the local environment, which includes extracellular matrix (ECM)[1]. This vasculogenic process is inextricably linked to subsequent primitive hematopoiesis, i.e., formation of the first erythroid and myeloid cells [2], implying a close lineage relationship between the first vascular endothelial and blood cells. The relevant $Flk1^+$ hematoendothelial progenitor cells arise from mesodermal precursors at gastrulation [3], migrate from the primitive streak, and aggregate in blood islands in the proximal extra-embryonic yolk sac on the seventh day of gestation (E7) in mouse embryos [4, 5]. Several key transcription factors and soluble effectors of vasculogenesis/angiogenesis and hematopoiesis are known [1]. Although ECM and ECM-derived proteolytic fragments are recognized as angiogenesis regulators [6] and sulfated glycosaminoglycans can promote endothelial differentiation of mesenchymal stem cells [7], much remains unknown about the influence of ECM on vasculogenesis. Another early cell lineage, primordial germ cells, are accompanied by a protective “traveling niche” of steel factor/stem cell factor-producing cells during migration to the gonads [8]. Whether a cell-associated ECM supports other early lineages such as hematoendothelial progenitors is unknown.

ECM surrounds all mammalian cells, forming a distinct pericellular matrix in some cell types, and the interstitial matrix of tissues. It influences cell behavior by modulating cell adhesion, migration and tissue mechanics, sequesters growth factors and cytokines, and its proteolysis can generate bioactive fragments. Proteoglycans, which are ECM and cell-surface molecules with one or more glycosaminoglycan chains covalently attached to a core protein, participate in all these mechanisms. For example, chondroitin sulfate proteoglycans (CSPGs) such as versican, which are bulky and inherently anti-adhesive, regulate focal adhesions and cell migration [9-11]. Heparan sulfate proteoglycans (HSPGs) sequester growth factors, including angiogenic growth factors such as $VEGF_{165}$ and FGF2 through their HS chains and act as co-receptors in angiogenic

signaling [12]. CSPGs can also bind $VEGF_{165}$ and may overlap functionally with HSPGs in VEGF-induced sprouting angiogenesis [13], but physiological in vivo contexts for this regulatory activity remain unidentified.

Versican is a widely distributed CSPG that aggregates with the glycosaminoglycan hyaluronan (HA), through its N-terminal G1 domain [14-17]. Its C-terminal G3 domain binds to ECM components fibronectin, fibrillins and tenascins [18] and was shown to interact with $VEGF_{165}$ in biochemical assays [19]. HA is anchored to cell-surface receptors such as CD44 and RHAMM as well as the membrane-localized hyaluronan synthases [20], providing a means by which versican can localize to the pericellular matrix. Pericellular versican was previously shown to modulate smooth muscle cell differentiation via regulation of cell adhesion [9, 21, 22]. Four versican isoforms (V0, V1-V3) arise from alternative splicing of large exons, numbered 7 and 8, encoding CS-bearing domains GAGα and GAGβ, respectively [16, 23]. A versican insertional mutant mouse allele (*Vcan*^{hdf}), which lacks all isoforms, demonstrated an essential role for versican in early cardiac development [24, 25]. *Has2* null embryos, lacking the major HA synthase, also die by 10 days of gestation with similar cardiac defects as *Vcan*$^{hdf/hdf}$ [26], consistent with the versican-HA complex being a major constituent of cardiac jelly. Here, upon identification of abnormal vasculature in *Vcan*$^{hdf/hdf}$ yolk sac, we investigated its role in vasculogenesis and early hematopoiesis, with investigation of the key findings in embryos with inactivation of hyaluronan synthase (*Has*) genes. An intimate association of versican and HA with $Flk1^+$ hematoendothelial progenitor cells from their origin at gastrulation is demonstrated to have profound significance for vasculogenesis and primitive hematopoiesis.

Results

Vcan$^{hdf/hdf}$ yolk sacs lack a vascular plexus:

Vcan$^{hdf/hdf}$ embryos did not survive past E10.5, and were recognizable by consistently smaller size and dilated pericardial sac at E9.5 (Figure 1A, Supplemental Figure 1). Although major developmental milestones, including axial rotation of the embryo and initiation of cardiac

contraction were completed by E9.5, *Vcan*$^{hdf/hdf}$ yolk sacs and embryos were less vascular (Figure 1B,C). Whole mount CD31 immunostaining revealed the lack of a vascular network in E9.5 *Vcan*$^{hdf/hdf}$ yolk sacs, in place of which scattered vascular CD31+ cells were present instead (Figure 1C).

In E9.5 wild-type yolk sac, versican localized to the mesoderm, but no staining was present in *Vcan*$^{hdf/hdf}$ yolk sacs (Figure 1D). HA-binding protein (HAbp) staining overlapped with versican in wild-type yolk sac mesoderm but was absent in *Vcan*$^{hdf/hdf}$ yolk sacs (Figure 1D). Fibronectin immunostaining in contrast, showed increased intensity in *Vcan*$^{hdf/hdf}$ yolk sacs, whereas collagen IV staining was unaffected (Figure 1D), suggesting that loss of HA did not represent global ECM reduction in *Vcan*$^{hdf/hdf}$ yolk sacs. Similar to *Has2*, *Itga5* and *Fn1*-null alleles, which have failed yolk sac vasculogenesis and hematopoiesis [26, 27], *Vcan*$^{hdf/hdf}$ yolk sacs consistently showed mesoderm detachment from visceral endoderm with few evident blood islands (Figure 1D, Supplemental Figure 2A-C). Intense F-actin staining was consistently observed in *Vcan*$^{hdf/hdf}$ visceral endoderm (Figure 1 D, Supplemental Figure 2A), and rounded, rather than spindle-shaped nuclei were observed in the yolk sac mesothelial layer (Supplemental Figure 2B). Transmission electron microscopy (TEM) undertaken with fixation conditions that preserved cell-matrix interactions [28] showed complete coverage of blood islands by vascular endothelium in wild-type yolk sac but discontinuous vascular endothelial cells with numerous membrane protrusions in *Vcan*$^{hdf/hdf}$ yolk sacs (Supplemental Figure 2C). Thus, versican is essential for proper yolk sac morphogenesis.

E8.5 *Vcan*$^{hdf/hdf}$ embryos had a normal shape, but appeared pale and their yolk sacs lacked a visible vascular network (Figure 2A). Whole-mount CD31 immunostaining of E8.5 embryos identified severe, widespread attenuation of vasculature (Figure 2B). *En face* imaging of whole-mount wild-type yolk sac stained with anti-CD31 demonstrated a well-formed vascular plexus which was lacking in *Vcan*$^{hdf/hdf}$ yolk sacs (Figure 2C). Immunostaining of versican and CD31, together with HA-staining in E8.5 wild-type yolk sacs revealed versican and HA co-localization

in patches corresponding to individual cells on the mesothelial aspect of blood islands (Figure 2D). mRNA *in situ* hybridization with *Vcan* exon 7 (GAGα), or exon 8 (GAGβ)-specific probes revealed that only the exon 8 probe hybridized to E8.5 yolk sac mesoderm (Figure 2E), suggesting exclusively versican V1 isoform expression at E8.5. Both *Vcan* probes hybridized strongly to E8.5 wild-type hearts (Figure 2F) but not *Vcan*$^{hdf/hdf}$ hearts (e.g., exon 8 probe, Figure 2G), indicative of specificity.

Versican and HA are associated with yolk sac Flk1^{+} cells

Flk1, a well characterized hematoendothelial progenitor marker indispensable for both vascular and blood lineage development [29], showed complete overlap with versican and HA on the mesothelial aspect of blood islands in wild-type E8.5 yolk sac (Figure 3A). *Vcan*$^{hdf/hdf}$ yolk sacs, in contrast, showed small blood islands with dramatically attenuated HA and Flk1 staining (Figure 3A). *En face* confocal microscopy of whole-mount wild-type E8.5 yolk sacs revealed discrete patches of versican throughout the mesoderm (Figure 3B). CD41, which is expressed upon specific commitment to the blood lineage [30], was detected in blood islands in the mid-mesoderm plane in wild-type yolk sacs (Figure 3B). Versican did not precisely overlap with CD41+ cells and was restricted to intense patches corresponding to individual endothelial cells in wild-type yolk sacs, evident both in the surface (mesothelial) plane and cross-sections, whereas *Vcan*$^{hdf/hdf}$ yolk sacs lacked CD41-stained blood islands entirely (Figure 3B). High magnification images showed a few cells with weak CD41 staining in *Vcan*$^{hdf/hdf}$ yolk sac mesoderm (arrowheads in Figure 3B), contrasting with well-demarcated CD41+ wild-type blood islands. Combined, these results show that versican and HA distribution at E8.5 is specifically associated with uncommitted Flk^{+} hemogenic endothelial cells, which are crucial for both blood and vascular development in the mouse embryo. However, versican and HA are not specifically associated with subsequently differentiated blood cells (Figure 3 B,C).

Versican is required for blood island formation

RT-qPCR revealed significantly lower *Flk1* expression in *Vcan*$^{hdf/hdf}$ yolk sac and

embryos (Figure 3D), in agreement with reduced Flk1 staining observed in the *Vcan*$^{hdf/hdf}$ mutants (Figure 3A). Neither expression of *Brachyury*, a mesoderm marker, nor *Has2*, encoding the major HA synthase in the embryo, were altered in *Vcan*$^{hdf/hdf}$ yolk sac or embryos (Figure 3D). Expression of genes encoding blood lineage commitment markers *Itga2b* (CD41) and *Runx1* were similarly reduced in the *Vcan*$^{hdf/hdf}$ yolk sacs and embryos, as well as erythroid and myeloid transcripts *Hbb* (β-globin), *Gata1* and *Ptprc* (CD45) (Figure 3D). CD31 (*Pecam1*) mRNA expression was greatly reduced in the *Vcan*$^{hdf/hdf}$ yolk sacs and embryos (Figure 3D), consistent with the observed lack of vasculature (Figure 2B). Methylcellulose colony formation assays demonstrated fewer colony-forming units (CFUs) in E8.5 *Vcan*$^{hdf/hdf}$ embryos and yolk sacs (Figure 3E), in agreement with fewer CD41-stained blood islands observed in the mutant yolk sacs.

Versican and HA are associated with the earliest Flk1$^+$ cells at gastrulation

Since Flk1$^+$ cells arise at gastrulation, we analyzed versican and HA distribution in wild-type E7.5 mouse embryos. Versican and HA co-localized to the extraembryonic mesoderm in the blood island ring (Figure 4 A,B), and colocalized with Flk1$^+$ cells (Figure 4 C,D). Correspondingly, RNA *in situ* hybridization of serial sections from several embryos showed consistent overlap between *Vcan*-, *Has2*- and *Flk1*-expressing cells in the extraembryonic mesoderm (Figure 4E, Supplemental Figure 3). *Vcan* exon 7-containing probes gave a weaker signal than exon 8 probes. In contrast, *Runx1*, which identifies blood lineage-committed cells, was expressed by cells in the extraembryonic mesoderm distinct from those expressing *Flk1*, *Vcan* and *Has2* (Figure 4E, Supplemental Figure 3). Thus, versican-HA ECM is intimately associated with the hematoendothelial lineage emerging at gastrulation.

Data mining of a single cell RNA sequencing (scRNA-seq) atlas of early (6.5 to 8.5 day-old) mouse embryos [31] supported specific *Vcan* expression by Flk1$^+$ hematoendothelial progenitors. High *Vcan* expression was first detected in hematoendothelial progenitors emerging at E6.75, as well as in nascent and uncommitted mesoderm (Supplemental Figure 4A-C). *Vcan* was expressed in *Kdr* (encoding *Flk1*)-expressing cells at E6.75, E7.0 and E7.5,

spanning mouse gastrulation (Supplemental Figure 4A-C). *Kdr*$^{+}$ cells also expressed *Has2* and the gene encoding the HA receptor, CD44 (Supplemental Figure B). These observations suggest a potential cell-autonomous role for versican in Flk1^{+} cells, bound to HA and thus potentially localized to their pericellular matrix via CD44 and HAS2. After E7.5 (e.g., at E 8.5), *Vcan* was broadly expressed in mesoderm, the developing brain, allantois and cardiomyocytes (Supplemental Figure 4C) and *Kdr* expression extended into endothelial cells, although hematoendothelial progenitors continued to express *Vcan* and *Kdr* subsequently (Supplemental Figure 4C). scRNA-seq data also showed that HA link proteins (*Hapln1-4*) were not expressed in hematoendothelial progenitors (Supplemental Figure 5A), and the major versican-binding link protein, HAPLN1, was not detected on immunostaining of E7.5 embryo sections (Supplemental Figure 5B). Staining for ADAMTS-cleaved versican (using anti-DPEAAE) revealed no staining in wild-type blood islands, suggesting that versican does not normally undergo proteolysis by ADAMTS proteases at this developmental stage (Supplemental Figure 5C).

Loss of versican dramatically reduces yolk sac and embryo HA levels

In addition to reduced HA staining in *Vcan*$^{hdf/hdf}$ yolk sac blood islands, we observed dramatic reduction of HAbp staining throughout *Vcan*$^{hdf/hdf}$ embryos (Figure 5A). Since *Has2* mRNA expression was unaltered in *Vcan*$^{hdf/hdf}$ embryos and yolk sacs (Figure 3D), reduced HAbp staining may have resulted from increased breakdown in situ, or alternatively, extraction of HA (which is water soluble) from tissue sections during staining. Therefore, fluorophore-assisted carbohydrate electrophoresis (FACE) [32-34] was undertaken on snap-frozen whole embryos to detect and quantify HA content (Figure 5B). HA-FACE showed reduction of HA compared to wild-type littermates, supporting HA loss intrinsically rather than during sample preparation (Figure 5B). In addition, FACE analysis demonstrated that versican is a major CSPG in E8.5 embryos, contributing nearly all unsulfated (0S) CS, since both the overall level of CS and its 0S form were dramatically reduced in *Vcan*$^{hdf/hdf}$ embryos (Figure 5B). Consistent with the role of versican and HA as an expansile complex, craniofacial mesenchyme and myocardium were severely

compacted in *Vcan*$^{hdf/hdf}$ embryos (Figure 5C). We also asked whether the absence of versican affected fibronectin, a major embryonic ECM component that is essential for angiogenesis and observed a dramatic increase both in fibronectin staining and mRNA in *Vcan*$^{hdf/hdf}$ embryos (Figure 5D, Supplemental Figure 6A,B), which is presently unexplained. In combination with unaltered *Has2* expression, these findings suggested increased HA turnover in *Vcan*$^{hdf/hdf}$ embryos. TMEM2 was recently identified as a major extracellular hyaluronan-depolymerizing enzyme [35-37]. RT-qPCR revealed significantly raised*Tmem2* expression in *Vcan*$^{hdf/hdf}$ yolk sac and embryos (Figure 5E). indicating that hyaluronan catabolism was activated in the absence of versican.

HA deficiency impairs vasculogenesis

Since HA was lost in the absence of versican, we inquired if the converse were true, and whether HA-deficiency indeed led to defective vasculogenesis, as previously suggested by morphology of *Has2* germline mutant yolk sac [26]. *Has2*$^{-/-}$ embryos die by E10 due to heart defects [26] whereas *Has1*$^{-/-}$ and *Has3*$^{-/-}$ mice are both viable and do not exhibit noticeable embryonic phenotypes [38, 39]. To completely deplete HA from developing embryos, we generated triple knockout embryos (*TKO*) lacking all three *Has* genes (*Has1*$^{-/-}$*; Has2*$^{-/-}$*; Has3*$^{-/-}$; referred to as *Has1-3*^{TKO}). We generated HA-deficient mouse embryos by intercrossing *Has1+3*$^{-/-}$*; Has2*$^{+/-}$ mice, as well as by epiblast-specific conditional deletion of *Has2* using *Sox2*-Cre mice. At E9.5, *Has1-3*^{TKO} embryos, like *Vcan*$^{hdf/hdf}$ and *Has2*-null embryos [26] showed loss of yolk sac vasculature (Figure 6A). HA staining in the *Has1-3*^{TKO} yolk sac and embryos was absent and the sections also showed a near-complete lack of versican staining (Figure 6B,C). In contrast, immunostaining for cleaved versican (anti-DPEAAE) showed robust and widespread versican processing in the absence of HA (Figure 6 B,D). Epiblast-specific *Has2* conditional deletion (*Sox2*-Cre; *Has2*$^{Fl/Fl}$) showed a similar loss of yolk sac vasculature and cardiac defects (Supplemental Figure 7A). RNA *in situ* hybridization showed a low level of *Has2* expression in these embryos and slightly reduced *Vcan* transcript levels (Supplemental Figure 7B). Phenocopying *Has1-3*^{TKO} embryos, the *Sox-2*Cre; *Has2*$^{Fl/Fl}$ embryos and yolk sacs showed loss of both HA and versican staining and increased ADAMTS-

mediated versican cleavage (Supplemental Figure 7C). Taken together, these data suggest that HA may protect versican from ADAMTS-mediated degradation.

Embryoid bodies formed by *Vcan*-null ES cells have impaired angiogenesis and hematopoiesis.

Since the dramatic loss of vasculature could result from perturbed hemodynamics due to cardiac defects in *Vcan*$^{hdf/hdf}$ embryos, we undertook an orthogonal in vitro approach for evaluation of versican in vasculogenesis and hematopoiesis. We used gene editing by CRISPR/Cas9 [40, 41] to introduce *Vcan*-null mutations in R1 mouse embryonic stem cells (mESC) [42]. *Vcan* exon 2 (containing the start codon) and exon 3 (start of the G1 domain) were targeted independently to obtain mESC clones D8 and F9 respectively, each with defined frameshift mutations that generated null alleles (Figure 7A). Since exons 2 and 3 are included in all *Vcan* splice isoforms, no versican was produced, as shown by western blot with anti-GAGβ antibody (Figure 7B). The mutated clones retained normal expression of *Oct4, Sox2, Nanog* and *C-myc* (Figure 7C) indicating unaltered pluripotency, validating their suitability for *in vitro* differentiation. *Vcan*-null and wild-type ES cells were allowed to form embryoid bodies (EBs), in which random differentiation into various lineages occurs. RT-qPCR analysis of *Has2* showed no change in *Vcan*-null EBs (Supplemental Figure 8A) while the mesoderm differentiation marker *Brachyury/T* showed a significant decrease in the F9 but not the D8 *Vcan*-null EBs (Supplemental Figure 8B). Similar to *Vcan*$^{hdf/hdf}$ embryos, *Vcan*-null embryoid bodies showed reduced *Kdr* expression (Supplemental Figure 8C), and the blood lineage commitment markers *Itga2b* (CD41) and *Runx1* (Supplemental Figure 8D), as well as of differentiated blood and vascular endothelial markers (Supplemental Figure 8 E,F). Since EB differentiation is random and independent of a closed pulsatile circulation, the data from embryoid bodies and the mutant mice together suggests that versican acts directly on Flk1^{+} hematoendothelial progenitors rather than indirectly *via* abnormal cardiac development.

We evaluated the angiogenic and hematopoietic potential of *Vcan*-null ESC using additional approaches. Sprouting angiogenesis was induced by culturing 4-day differentiated EBs in 3-dimensional collagen I gels and treatment with VEGF-A_{165} for 12 days [43]. Robust sprouts positive for CD31 and smooth muscle α-actin staining were seen in wild-type EBs, but not in the majority of *Vcan*-null EBs (Figure 7D,E). The few *Vcan*-null EBs with sprouting had fewer sprouts per EB, and these were significantly shorter than wild-type sprouts (Figure 7F,G). When 10-day old EBs were disaggregated and the cells were plated in a 3-dimensional methylcellulose matrix containing a complete set of blood differentiation cytokines, significantly fewer blood colonies were formed by *Vcan* null EBs (Figure 7H).

The versican-HA complex sequesters growth factors essential for vasculogenesis and primary hematopoiesis.

These observations raised questions about the underlying mechanisms by which the versican-HA matrix supported $Flk1^+$ cells. To investigate this, we turned to an *ADAMTS9* null RPE1 cell line (D12) which lacks two key versican-degrading proteases, ADAMTS9 and ADAMTS20 [22]. Although RPE1 cells are not relevant to hematoendothelial progenitors, they were chosen for the relevance of their matrix, which demonstrates constitutively strong versican staining as a result of reduced ADAMTS activity, in order to determine how versican may modulate vasculogenesis (Figure 8A). HAbp staining of these cells demonstrated stronger HA staining than wild type RPE1 cultures, with formation of long HA-stained cables decorated with versican (Figure 8A, Supplemental Figure 9A,B). Such cables were previously noted to occur in the presence of 25 mM glucose-containing medium, which was used here [44] [45]. RT-qPCR revealed reduced *HAS2* & *HAS3* expression in RPE-1 D12 cells compared to wild-type (Figure 8B) with no change in *HAS1* expression and drastic reduction of *TMEM2* expression was observed (Figure 8B). Upon siRNA-mediated versican depletion [46, 47], RPE1-D12 cells showed dramatically reduced versican and HA staining and absence of HA/versican cables (Figure 8C, Supplemental Figure 10A). Conversely, RT-qPCR showed increased *TMEM2* expression after *VCAN* knockdown

(Supplemental Figure 10B), suggesting upregulation of the HA-depolymerase *TMEM2* by reduction of versican as a possible mechanism of HA loss.

Next, to test if versican could sequester growth factors known to regulate vasculogenesis, we treated wild-type and RPE1-D12 cells with increasing concentrations of recombinant $VEGF_{165}$ and Ihh. Each showed dose-dependent punctate staining in RPE1-D12 monolayers which co-localized with the versican-HA cables, imaged by confocal fluorescent and super-resolution microscopy (Figure 8D, Supplemental Figure 11A-B, Supplemental Figure 12A-B). Upon *VCAN* mRNA depletion in RPE1-D12 cells, both $VEGF_{165}$ and Ihh staining were significantly reduced (Figure 8D). Enzymatic removal of proteoglycan chondroitin sulfate chains prior to addition of recombinant $VEGF_{165}$ and Ihh to D12 cultures dramatically reduced $VEGF_{165}$ and Ihh staining intensity without affecting versican core protein staining intensity or distribution (Figure 8E,F), suggesting that versican CS chains mediated VEGF and Ihh binding.

Discussion

Although versican is widely expressed during organogenesis and in adult tissues [14], the chronology of its expression in early vascular development undertaken here and independently derived from recently published single cell RNA-seq data, shows a specific association with $Flk1^+$ cells from their earliest origin in the gastrulating embryo until establishment of the yolk sac vasculature and primitive hematopoiesis. Analysis of *Vcan* mutant mice *in vivo* and *Vcan*-null embryoid bodies *in vitro* suggest that versican has an indispensable role in vasculogenesis and primitive hematopoiesis. Taken together, RNA *in situ* hybridization data, scRNA-seq analysis of $Flk1^+$ cells and immunostaining of embryos suggests that versican is a product of $Flk1^+$ cells that associates with them via HA and CD44 to form a crucial, possibly cell-autonomously acting pericellular ECM. Furthermore, in vitro analysis undertaken in RPE-1 D12 cells for their high versican levels, showed dose-dependent binding of VEGF and Ihh to the CS-chains of versican.

Two novel, unexpected findings of this study were the substantial loss of embryonic and extraembryonic HA in the absence of versican and reciprocally, of versican in the absence of HA.

Also unexpected, and presently unexplained, is the transcriptional effect of versican levels on TMEM2. As in *Vcan*$^{hdf/hdf}$ yolk sac, avascularity was previously noted in *Has2* null yolk sac [26], although it was not studied further. *Has2* and *Vcan* null cardiac defects are similar, which suggested that an obligate versican-HA complex in cardiac jelly and endocardial cushions was required for cardiac morphogenesis [24-26]. The present work similarly strongly suggests that a versican-HA complex, rather than versican alone, is necessary for vasculogenesis and primitive hematopoiesis (Figure 9). HA-versican aggregates have a net negative charge, and exert swelling pressure *via* absorption of water (the Gibbs-Donnan effect) [48]. As shown here and previously, embryonic tissues compact in their absence [24, 49]. Although versican-deficient yolk sac showed extensive structural disorganization at E9.5, it is clear that the association and effect of versican vis-à-vis Flk1$^+$ cells occurs much earlier, i.e., shortly after gastrulation. Previous work identified both versican and HA in association with mesoderm formed in vitro in embryoid bodies arising from mouse ES cells [50], as well as expression in human ES cells [51]. Reduced vasculogenesis, angiogenesis and hematopoiesis in *Vcan*-null embryoid bodies supports a direct, local role of versican on hematoendothelial progenitors rather than a secondary effect of cardiac anomalies on vasculogenesis, or of yolk sac disorganization on blood island formation. We therefore conclude that versican-HA aggregates act directly and as early as E6.75 within the microenvironment of Flk1$^+$ cells.

HA, which is extruded directly from HA synthases on the plasma membrane, is decorated with versican, and retained at the cell surface via HA synthases or CD44 and other HA receptors [52]. *Cd44* is coordinately expressed with *Vcan* and *Has2* by Flk1$^+$ cells during early embryogenesis. Nevertheless, *Cd44* null mice survive and are not known to have vasculogenesis or primitive erythropoiesis defects [53], suggesting that HAS2 acting as a *de facto* receptor, may participate in forming a cell-associated versican-HA complex. The versican-HA pericellular matrix has a well-established impact on different cells. We previously found that the amount of versican in the pericellular matrix of fibroblasts and vascular and myometrial smooth muscle cells [9, 21,

54] was a determinant of phenotype modulation. Versican is anti-adhesive [9, 54], which may allow Flk1$^+$ cells to migrate and proliferate efficiently after their emergence at gastrulation. Another possible role of versican-HA is sequestration of vasculogenic factors such as VEGF-A and Ihh. Versican binding to VEGF-A_{165} and Ihh *via* its CS-chains (this study) or G3 domain [19], may generate high concentrations around Flk1$^+$ cells. Versican is associated with Flk1$^+$CD41$^-$ cells, but not with the Flk1$^-$CD41$^+$ yolk sac cells subsequently, suggesting that the versican-HA-rich pericellular ECM specifically regulates the fate of Flk1$^+$ CD41$^-$ cells. We conclude that as the dominant CSPG in the embryo, specifically localized to the vicinity of Flk1$^+$ cells, versican may sequester essential factors such as VEGF-A and Ihh to provide a high local concentration that sustains the Flk1$^+$ population.

Although lack of versican led to higher *Fn1* expression, *Vcan*$^{hdf/hdf}$ defects are unlikely to result from excess fibronectin, because previous work has shown that deficiency, not excess of fibronectin or the fibronectin receptor subunit α5 integrin results in reduced embryo and yolk sac vascularity [27, 55]. Since versican binds fibronectin through the G3 domain [19], we conclude that the three major components of the provisional embryonic ECM (versican, HA and fibronectin) are each crucial for establishment of the first blood vessels in the embryo. In the absence of versican, the HA catabolism rate *via* upregulated TMEM2 likely exceeds the HA synthesis rate. It was previously noted that HA deposition was reduced to 85% of normal in fibroblasts taken from a mouse hypomorphic *Vcan* mutant (*Vcan*$^{\Delta3/\Delta3}$) having 75% reduction of versican [56]. In association with reduced HA deposition, *Vcan*$^{\Delta3/\Delta3}$ fibroblasts had accelerated senescence, suggesting a possible mechanism for the lack of Flk1$^+$ cells in *Vcan*$^{hdf/hdf}$ yolk sac, although this study did not specifically address the fate of Flk1+ cells.

The data suggested stronger association of exon 8-containing *Vcan* transcripts than exon 7-containing transcripts with blood islands at gastrulation, and exon 7 transcripts were absent at E8.5. Autosomal dominant splice site mutations affecting exon 8 (leading to its exclusion) and exon 8 deletions in humans cause Wagner syndrome [57-59], which is characterized by impaired

vision and defects of the ocular vitreous and retina, but lacks consistent extra-ocular manifestations. Exon 7 inactivation in mice led to specific neural anomalies and subtle cardiac anomalies [60, 61]. Thus, neither individual exon mutation in mice or humans is associated with embryonic lethality, defective vasculogenesis or impaired hematopoiesis. We conclude that both exon 7 and exon 8-containing transcripts, possibly included in V0, the transcript containing both exons, are required for vasculogenesis and hematopoiesis.

The GAGβ domain encoded by exon 8 has a unique N-terminal sequence, which is cleaved by ADAMTS proteases at the E^{441}-A^{442} peptide bond in several contexts, notably cardiac valve development, interdigital web regression, umbilical cord development, neural tube and palate closure and myometrial activation [9, 22, 62, 63]. The resulting N-terminal versican V1 fragment, G1-$DPEAAE^{441}$, named versikine, has bioactivity in interdigital web regression and myeloma growth [64, 65]. However, *Vcan* knock-in mouse mutants in which E^{441}-A^{442} was mutated to render it uncleavable can complete gestation and have normal yolk sac avascularity, suggesting that E^{441}-A^{442} cleavage is not involved in hematoendothelial development ([66] and Nandadasa et al., manuscript in preparation).

Both phylogenetically and ontogenetically, basement membranes are accepted to be the earliest organized matrices formed, and indeed, basement membrane components such as laminins have a well-established significance for maintenance of stemness and for epiblast organization [67-69]. The versican-HA matrix appears to be a later evolutionary innovation, and our data suggests that it may be representative of a second wave of matrix expansion and utilization for cellular regulation during mammalian evolution. With the roles in vasculogenesis and hematopoiesis elucidated here, and given their established significance for cardiac development, it is not an exaggeration to state that the versican-HA matrix is crucial for development of the entire circulatory system. Indeed, versican-HA matrix may also have a broad role in formation of vasculature by angiogenesis in other physiological and disease settings. Recent work found that syngeneic B16F10 tumors in adult $Vcan^{hdf/+}$ mice had significantly

impaired angiogenesis and reduced growth [70]. Relevant to the overlap of versican-HA with Flk1 expression, a recent study utilizing syngeneic B16F10 tumors in *Flk1*$^{+/-}$ mice also found reduced angiogenesis during tumor growth [71]. Furthermore, VEGF binding of the versican-HA ECM which is quantitatively increased in the presence of high glucose, may be relevant to diabetic retinopathy, a common complication of diabetes where the increased activity of VEGF is well-established and indeed, a current target of treatment [72].

Methods

Mice

Vcan$^{Tg(Hoxa1)1Chm}$ (*Vcan*^{hdf}) mice [25] (Supplemental Figure 1) were obtained under a material transfer agreement from Roche. Generation of *Has1*$^{-/-}$; *Has3*$^{-/-}$ double knockout mice was described previously [73]. A *Has2*-null allele (*Has2*$^{-}$) was created from a *Has2*^{flox} allele [74] by crossing *Has2*$^{flox/flox}$ mice with the germline deleter *Meox2-Cre* mice [75]. All of these mouse lines were backcrossed to C57BL/6J for more than 10 generations. *Has1*$^{-/-}$; *Has2*$^{+/-}$; *Has3*$^{-/-}$ mice were bred from these mutant mice. Triple *Has* knockout (TKO) embryos were generated by crossing *Has1*$^{-/-}$; *Has2*$^{+/-}$; *Has3*$^{-/-}$ female and male mice. In a second approach to generate HA-deficient mouse embryos, *Has2*$^{Fl/Fl}$; *Sox2Cre*^{tg} mice were generated by crossing *Has2*$^{Fl/Fl}$ males with *Has2*$^{+/Fl}$; *Sox2Cre*^{tg} females. Mouse experiments were conducted with IACUC approval (Cleveland clinic protocols 2015:1530 and 2018:2045). Mice were maintained in a fixed light-dark cycle with food and water *ad libitum*. For genotyping E8.5 embryos with intact yolk sacs, the allantois was dissected out and lysed in 10 μl DirectPCR (Tail) digest reagent (Qiagen, catalog no. 102-T) supplemented with 1 μl of proteinase K overnight at 55°C. Tails were used to genotype E9.5 embryos. *Vcan*^{hdf} and wild-types were identified with a specific genotyping strategy based on the genetic interruption (Supplemental Figure 1). Details of the *Has1-3* mutant mouse genotyping is provided in the Supplemental Methods. *Vcan*$^{hdf/hdf}$ embryos were compared to wild-type littermates in all experiments.

Mouse embryonic stem cell (mESC) culture.

R1 mESC [42] (Case Transgenic and Targeting Facility) were cultured on 0.3% type B gelatin (Sigma-Aldrich, catalog no. G9382) coated 60 mm cell culture plates in Iscove's Modified Dulbecco's Medium (IMDM) containing 4mM L-glutamine and 1mM sodium pyruvate, supplemented with 20% fetal bovine serum (Hyclone, catalog no. SH30071), 0.1 mM cell culture grade 2-mercaptoethanol (Gibco, Life Technologies, catalog no. 21985), 0.1mM nonessential amino acids (Gibco, Life Technologies, catalog no. 11140-050), 50 μg/mL penicillin/streptomycin and $1x10^6$ units/mL leukemia inhibitory factor (LIF; ESGRO, EMD Millipore, catalog no. ESG1106) in a humidified 5% CO_2, 37°C environment. mESC were maintained at 60-80% confluence, with daily medium change and passaged every other day in a 1:5 split.

CRISPR/Cas9 targeting of mESC *Vcan*

2.5 μg of CRISPR/Cas9 plasmids in the U6gRNA-Cas9-2A-GFP vector, targeting *Vcan* exon 2 or exon 3 (Sigma-Aldrich, target IDs MM0000080027 and MM0000080028) were transfected into R1 mESCs at 60-80% confluence in 6-well plates coated with 0.3% gelatin, using FuGene 6 (Promega, catalog no. E2691). 24 hrs post-transfection, individual GFP+ mESCs were sorted into 96-well plates coated with 0.3% gelatin using a FACSAria-II cell sorter (BD Biosciences). Fast-growing wells (containing >1000 cells/well) were trypsinized and expanded to 24-well cell culture plates after 7-10 days. Culture medium was replaced daily. Genomic DNA from clones was isolated using DirectPCR (Tail) reagent (Viagen, catalog no. 102-T) and *Vcan* exon 2 and exon 3 were amplified using Phusion *Taq* (NEB, catalog no. F530L) (see SI). Amplicons were excised from 2% agarose gels, purified using the QIAquick Gel Extraction kit (QIAGEN, catalog no. 28704) and cloned into pCR-Blunt II-TOPO vector using the Zero blunt PCR cloning kit (Life Technologies, Invitrogen, catalog no. K2800-40). Plasmid DNA was harvested from bacterial colonies for Sanger-sequencing to determine the precise mutations. Two independent *Vcan*-null mESC clones, D8 and F9, were established. Western blotting and immunostaining of 10-day old

433 embryoid bodies from these lines (see below) confirmed *Vcan* inactivation. Embryoid body
434 formation and induction of vascular sprouts is described in the Supplemental Methods.

435 **Immunostaining and fluorescence microscopy**

436 Immunostaining of E 9.5 and E 8.5 yolk sac was carried out on 30 μm thick vibratome sections
437 [22] or paraffin-embedded 7 μm sections. Immunostaining of collagen-embedded embryoid
438 bodies were carried out in 4-chamber cell culture slides (Fisher Scientific, catalog no. 354114).
439 Confocal microscopy images of whole-mount mouse embryos and sections were acquired using
440 a Leica TCS SP5 II multiphoton confocal microscope equipped with a 25X water immersion
441 objective (Leica Microsystems, Wetzlar, Germany). For 3D-projection of whole-mount Z-stacks,
442 the Volocity 3D imaging software was used (version 6.3, PerkinElmer, Inc., Waltham, MA) in
443 maximum intensity projection method.

444 **Methylcellulose colony formation assay**

445 Single cell suspensions of E8.5 embryos, yolk sacs or day-10 embryoid bodies were generated
446 by incubation with trypsin for 10 minutes followed by disaggregation by pipetting with a 200 μL
447 pipette tip until complete. 50,000 cells from each experimental group were transferred to a single
448 35 mm culture dish containing 1 mL of MethoCult GF M3434 culture medium (Methylcellulose
449 medium with recombinant cytokines for mouse cells, Stem Cell Technologies, Vancouver, CA,
450 catalog no. 03434) using a 3 mL syringe and 16-gauge needle, following the manufacturer's
451 protocol. Triplicate cultures from each genotype were incubated for 14 days in a humidified, 5%
452 CO_2, 37°C cell culture incubator. Blood colonies were counted using an inverted microscope.
453 Aggregates with >50 cells were considered a colony-forming unit (CFU).

454 Additional details of reagents and procedures including primary antibodies used,
455 RNAscope in situ hybridization, western blotting, transmission electron microscopy, and
456 fluorophore-assisted carbohydrate electrophoresis (FACE) are described in the Supplemental
457 Methods

Acknowledgments

This work was supported by the NIH-NHLBI Program of Excellence in Glycosciences award HL107147 (to S.S.A., R.J.M.,), by the Allen Distinguished Investigator Program, through support made by The Paul G. Allen Frontiers Group and the American Heart Association (award 17DIA33820024 to S.S.A), NIH RF1 AG057579 (to Y.Y.) and the David and Lindsay Morgenthaler Postdoctoral Fellowship and the Mark Lauer Pediatric Research grant (to S.N.). Purchase of the Leica SP8 confocal microscope was supported by NIH SIG grant 1S10RR026820-01. We thank Dr. David LePage and Dr. Ron Conlon at the Case Transgenic and Targeting Facility for R1 mES cells, Eric Schultz and Joseph Gerow of the LRI Flow Cytometry Core for mES cell sorting, Valbona Cali for FACE assays, Dr. Judy Drazba and Mei Yin of the LRI Imaging Core for guidance with confocal and electron microscopy and the Apte laboratory members for valuable discussions.

Declaration of interests

The authors declare no competing interests

Figure Legends

Figure 1. *Vcan*$^{hdf/hdf}$ yolk sacs are avascular and lack hyaluronan.

(A) E9.5 wild type and *Vcan*$^{hdf/hdf}$ embryos. The red arrowhead shows the dilated pericardial sac in the mutant.

(B) E9.5 yolk sacs imaged in situ demonstrate the absence of vasculature in the E9.5 *Vcan*$^{hdf/hdf}$ yolk sac.

(C) Three-dimensional (3D) maximum-intensity projections of whole-mount yolk sacs stained with anti-CD31 (red) showing absence of the vascular network in E9.5 *Vcan*$^{hdf/hdf}$ yolk sacs (n=3 yolk sacs of each genotype).

(D) Versican GAGβ staining (green) is present throughout the mesoderm (Me) of E9.5 wild type yolk sacs and absent in the *Vcan*$^{hdf/hdf}$ yolk sac. F-actin (red) staining highlights visceral endoderm

(VE) detached from mesoderm in *Vcan*$^{hdf/hdf}$ yolk sacs. HA and fibronectin (green) were similarly distributed as versican in wild type yolk sac, but HA staining was absent in *Vcan*$^{hdf/hdf}$ yolk sac and fibronectin staining was more intense. Collagen IV staining intensity was similar in wild type and *Vcan*$^{hdf/hdf}$ yolk sacs (n=3 yolk sacs of each genotype). Scale bar in A, B=1mm, C= 100μm, D= 50μm.

Figure 2. Impaired vasculogenesis in the *Vcan*$^{hdf/hdf}$ embryo and yolk sac.

(A) E8.5 *Vcan*$^{hdf/hdf}$ yolk sacs are avascular yet embryos dissected out of the yolk sac appear morphologically similar to wild type.

(B) Maximum intensity projections of whole mount E8.5 wild type and *Vcan*$^{hdf/hdf}$ embryos stained with anti-CD31 (red) and DAPI (blue). Boxed areas are shown at higher magnification with the red channel only in the lower panels. Residual wild-type yolk sac is marked by a white dotted line (n=3 embryos from each genotype).

(C) Three-dimensional (3D) maximum intensity projections of yolk sacs stained *en face* with anti-CD31 (red) show a well-formed vascular plexus in wild type yolk sac and disorganized CD31+ cells in *Vcan*$^{hdf/hdf}$ yolk sac (n=3 yolk sacs from each genotype).

(D) Cross section of E8.5 wild type yolk sac blood islands co-stained with versican (green), HAbp (red) and CD31 (white). Versican and HA co-localize with CD31+ cells on the mesothelial aspect of blood islands (arrowheads). The blood island imaged on the left is enlarged in the bottom right-hand panel (n=3 wild type yolk sacs). VE, visceral endoderm, Bi, blood island,

(E) RNAscope in situ hybridization of E8.5 wild-type yolk sac shows expression of *Vcan* isoforms containing exon 8 (V0,V1), but not exon 7 (V0, V2) in mesoderm adjacent to blood islands (Bi), VE, visceral endoderm.

(F) *Vcan* exon 7 and exon 8 probes both hybridize to myocardium (Mc) of E8.5 wild-type embryos. En, Endocardium.

(G) *Vcan* probes (exon 8 shown) do not hybridize to *Vcan*$^{hdf/hdf}$ heart. Scale bar in **D**=10μm, **E**= 25μm, 50μm in **F-G**.

Figure 3. Versican and HA localize to Flk1+ cells and are essential for yolk sac blood island formation.

(A) E8.5 wild type and *Vcan*$^{hdf/hdf}$ yolk sac cross-sections co-stained with versican (magenta), HAbp (red) and Flk1 (green). In wild type yolk sac, versican-HA staining colocalizes with Flk1. In *Vcan*$^{hdf/hdf}$ yolk sac, blood islands (Bi) are smaller and both HAbp staining and Flk1 staining are weak. Arrowhead: versican-HA-Flk1 co-stained patches, asterisks: cell shown at higher magnification in the right-hand panels (n=4 yolk sacs from each genotype). VE, visceral endoderm.

(B) *En face* confocal imaging of E8.5 yolk sac versican (red) and CD41 (green) staining with the mesothelial aspect facing the objective (bottom). Surface optical sections show versican-rich foci throughout wild type yolk sac that are absent in *Vcan*$^{hdf/hdf}$ yolk sac. The mid-optical image shows versican and CD41 co-stained cells in blood islands. Versican is associated with wild-type blood islands but does not overlap with CD41. No CD41+ cells were observed in *Vcan*$^{hdf/hdf}$ yolk sac. The higher magnification image shows the distinct cell populations marked by versican and CD41. Arrowheads mark weak CD41 staining in *Vcan*$^{hdf/hdf}$ images (n=3 yolk sacs from each genotype).

(C) Cross-section of an E8.5 wild type blood showing no overlap of HA (red) and CD41 (green) (n=3 yolk sacs).

(D) qRT-PCR analysis of wild type and *Vcan*$^{hdf/hdf}$ yolk sacs and embryos shows significantly lower *Flk1* expression but not *Has2* or *Brachyury* expression in *Vcan*$^{hdf/hdf}$ mutants. CD41 *(Itga2b)* and *Runx1* expression were significantly lower in *Vcan*$^{hdf/hdf}$ yolk sac and embryos. Blood markers β-*globin*, *Gata1* and CD45 (*Ptprc*) and the vascular endothelial marker CD31 (*Pecam1*), were

reduced in *Vcan*$^{hdf/hdf}$ yolk sacs and embryos (n=3 yolk sacs and embryos from each genotype, error bars= S.E.M., *, p<0.05; **, p<0.01; ***, p<0.001).

(E) Methylcellulose assay shows significantly fewer blood colony-forming units (CFUs) in *Vcan*$^{hdf/hdf}$ yolk sacs and embryos (n=3 yolk sacs and three embryos from each genotype, error bars= S.D.,*, p<0.05; **, p<0.001). Scale bars=25μm in **A**, 100μm and 20μm in **B.**

Figure 4. Versican and HA co-localize with Flk1+ cells from their origin at gastrulation.

(A) Maximum intensity projection image of an E7.5 embryo shows strong versican staining (green) in the putative blood island (BI) ring (white brackets) in the proximal extraembryonic (Exe) region. Emb, embryo.

(B-E) Serial sections of E7.5 wild type embryos analyzed by immunostaining **(B-D)**, or by RNAscope in situ hybridization **(E)**. **(B-C)** Versican (green) and HAbp (red) colocalize in extraembryonic mesoderm corresponding to the blood island ring (white brackets and arrowheads). The blood islands on the left are shown at high magnification in **(C-D)**. Arrowheads show colocalization of versican, HAbp and Flk1 in extraembryonic mesoderm (N=4 embryos). Epc, ectoplacental cavity; Ch, chorion; Exc, exocelomic cavity; Am, amnion; Ac, amnion cavity; Ne, neural ectoderm; Me, mesoderm; Ve, visceral endoderm.

(E) *In situ* hybridization for *Vcan* exon 7, *Vcan* exon 8, *Has2*, *Flk1* and *Runx1*. *Vcan* exon 8, *Has2* and *Flk1* mRNAs have near-identical expression patterns (red) corresponding to primitive streak cells migrating toward extra-embryonic mesoderm. *Vcan* exon 7 (GAGα) shows weaker overlapping expression. *Runx1* marks committed blood cells (n=4 embryos). Scale bars in **B,E**= 100μm.

Figure 5. *Vcan* inactivation results in loss of hyaluronan.

(A) Versican (green) and HAbp (red) staining of E8.5 wild type and *Vcan*$^{hdf/hdf}$ embryos showing severely reduced HAbp staining in *Vcan*$^{hdf/hdf}$ embryos. Arrowheads indicate versican and HAbp-stained yolk sac blood islands (n=3 embryos each genotype).

(B) *(Top)* Fluorophore-assisted carbohydrate electrophoresis (FACE) analysis for chondroitin sulfate (CS-FACE) and hyaluronan (HA-FACE) in E8.5 littermate embryos. Versican is the major CS-proteoglycan in E8.5 embryos. HA content is significantly reduced in *Vcan*$^{hdf/hdf}$ embryos. *(Bottom)* Quantification of CS and HA FACE, normalized to DNA (n=4 embryos from each genotype, error bars= S.E.M.,**, p<0.01; ***, p<0.001; ****, p<0.0001).

(C) 1 μm thick, toluidine blue-stained Eponate 12 sections from E8.5 wild type and *Vcan*$^{hdf/hdf}$ embryos showing compaction of craniofacial mesenchymal cells (Me) and loss of cardiac jelly (CJ) between the myocardium (Mc) and endocardium (En). The red line indicates the boundary of neural epithelium (NE) with mesenchyme (n=3 embryos each genotype).

(D) E8.5 wild *Vcan*$^{hdf/hdf}$ embryo sections stained with F-actin (red) and fibronectin (green) showing stronger fibronectin staining (n=3 embryos each genotype).

(E) RT-qPCR shows increased *Tmem2* mRNA in *Vcan*$^{hdf/hdf}$ embryos and yolk sacs (n=3 embryos and yolk sacs from each genotype, error bars= S.E.M., ***, p<0.001; ****, p<0.0001). Scale bar in **A**= 200μm, 50μm and 20μm in **C**.

Figure 6. Versican content is severely reduced in *Has1+2+3* null embryos.

(A) E9.5 *Has1+3* null embryos (control) and *Has1+2+3* null embryos showing the dilated pericardial sac in the latter (arrowhead) similar to *Vcan*$^{hdf/hdf}$ (n=3 embryos each genotype).

(B) *Has1+3* null yolk sac (control) and *Has1+2+3* null yolk sac co-stained with HAbp (green) and versican or cleaved versican (DPEAAE) (red) show loss of both HA and versican, although cleaved versican (DPEAAE, red, bottom) is present in *Has1+2+3* null yolk sac (n=3 yolk sacs each genotype).

(C-D) *Has1+3* null yolk sac (control) and *Has1+2+3* null embryos co-stained with HAbp and versican **(C)** or cleaved versican (DPEAAE) **(D)**, show loss of HA and versican staining and weaker DPEAAE staining in the *Has1+2+3* null embryos (n=3 embryos each genotype). Scale bars = 200μm in **C**,**D**.

Figure 7. Embryoid bodies (EBs) from *Vcan*-null mouse embryonic stem cells (mESCs) are poorly responsive to VEGF and form few blood colonies.

(A) *Vcan* locus showing targeting by independent guide RNAs (gRNAs) targeting exons 2 and 3. Scissors indicate the Cas9 cleavage site 3 bp from the protospacer adjacent motif (PAM, orange lettering). An exon 2 mutant mESC clone (D8) had a homozygous 1 bp insertion (bold red letters) and an exon 3 mutant clone (F9) had heterozygous targeting: deletion of T/A in one allele and a 19-bp deletion in the other, each resulting in frame-shifts.

(B) Western blot of 10-day differentiated EBs shows no versican in EBs derived from clones D8 and F9 (n=10 pooled embryoid bodies each group).

(C) RT-qPCR analysis showing unaffected expression of pluripotency markers *Oct4*, *Sox2*, *Nanog* and *C-myc* in D8 and F9 (n=3 independent batches of EBs from each genotype, error bars= S.E.).

(D) 4-day-old *Vcan*-null embryoid bodies embedded in collagen I and treated with $VEGF_{165}$ for 12 days have reduced vascular sprouting identified by CD31 (green) or α-SMA (red) immunostaining (n=3 independent batches of EBs from each genotype).

(E) D8 and F9 EBs show significantly fewer vascular sprouts (n=3 independent batches of EBs from each genotype, error bars= S.E. **, $p<0.01$; ***, $p<0.001$).

(F) Fewer sprouts/EB were seen in D8 and F9 EBs. (n=3 independent batches of EBs from each genotype, error bars= S.D., ***, $p<0.001$; ****, $p<0.0001$).

(G) Significantly shorter sprouts in *Vcan* null lines (n=3 independent batches of EBs from each genotype, error bars= S.D., ****, $p<0.0001$).

(H) Methylcellulose colony assay using dissociated 10-day old EBs shows significantly fewer colonies in *Vcan* null EBs. (n=3 independent batches of EBs from each genotype, error bars= S.D., **, p<0.01). Scale bar in **D** is 200 μm.

Figure 8. Versican regulates HA abundance and cable formation and sequesters VEGF and Ihh *via* chondroitin sulfate (CS) chains in a cell culture model.

(A) Increased versican (red) and HAbp staining (green) in *ADAMTS9*-deficient (D12) RPE-1 cells. Versican and HA co-stained cables are formed in D12 cells.

(B) RT-qPCR showing reduced *HAS2* and *HAS3* mRNA but not *HAS1* or *CD44* and dramatically reduced *TMEM2* expression in D12 cells. (n=3 independent RNA extractions, error bars= S.E.M., *, p<0.05; ****, p<0.0001).

(C) *VCAN* knockdown reduces both versican (red) and HA staining in D12 cells.

(D) Recombinant $VEGF_{165}$ or Ihh (green) co-staining with versican (red) in control siRNA-transfected D12 cells is lost in *VCAN* siRNA-transfected D12 cells.

(E) The schematic illustrates chondroitinase ABC removal of versican GAG chains and the experimental timeline used.

(F) Fluorescence microscope of VEGF and Ihh with versican, with or without chondroitinase ABC treatment prior to addition of recombinant $VEGF_{165}$ or Ihh (green) shows reduced binding of both growth factors after CS-chain removal, which does not affect versican core protein staining (red). Scale bars in **A** are 50μm and 100μm, 20μm in **D** and **F** and 50μm in **C-F**.

Figure 9. HA-versican pericellular matrix functions as an essential niche for Flk1+ cells. Model depicting the chronology of versican and HA expression and proposed functions in murine extraembryonic mesoderm during vasculogenesis and hematopoiesis. The present work localizes HA-versican to the pericellular matrix of Flk1+ cells, but not the downstream CD41+ committed

progenitors or to other CD31+ vascular endothelial cells. The inset box proposes that the negatively charged HA-versican pericellular matrix sequesters pro-vasculogenic factors such as VEGF and Ihh.

References:

1. Qiu, J. and K.K. Hirschi, *Endothelial Cell Development and Its Application to Regenerative Medicine.* Circ Res, 2019. **125**(4): p. 489-501.
2. Risau, W. and I. Flamme, *Vasculogenesis.* Annu Rev Cell Dev Biol, 1995. **11**: p. 73-91.
3. Lugus, J.J., et al., *Both primitive and definitive blood cells are derived from Flk-1+ mesoderm.* Blood, 2009. **113**(3): p. 563-6.
4. Ferkowicz, M.J. and M.C. Yoder, *Blood island formation: longstanding observations and modern interpretations.* Exp Hematol, 2005. **33**(9): p. 1041-7.
5. Dzierzak, E. and N.A. Speck, *Of lineage and legacy: the development of mammalian hematopoietic stem cells.* Nat Immunol, 2008. **9**(2): p. 129-36.
6. Red-Horse, K., et al., *Endothelium-microenvironment interactions in the developing embryo and in the adult.* Dev Cell, 2007. **12**(2): p. 181-94.
7. Lozito, T.P., et al., *Human mesenchymal stem cells express vascular cell phenotypes upon interaction with endothelial cell matrix.* J Cell Biochem, 2009. **107**(4): p. 714-22.
8. Gu, Y., et al., *Steel factor controls primordial germ cell survival and motility from the time of their specification in the allantois, and provides a continuous niche throughout their migration.* Development, 2009. **136**(8): p. 1295-303.
9. Mead, T.J., et al., *ADAMTS9-Regulated Pericellular Matrix Dynamics Governs Focal Adhesion-Dependent Smooth Muscle Differentiation.* Cell Rep, 2018. **23**(2): p. 485-498.
10. Perris, R., et al., *Inhibitory effects of PG-H/aggrecan and PG-M/versican on avian neural crest cell migration.* Faseb J, 1996. **10**(2): p. 293-301.
11. Yamagata, M., et al., *Regulation of cell-substrate adhesion by proteoglycans immobilized on extracellular substrates.* J Biol Chem, 1989. **264**(14): p. 8012-8.
12. van Wijk, X.M. and T.H. van Kuppevelt, *Heparan sulfate in angiogenesis: a target for therapy.* Angiogenesis, 2014. **17**(3): p. 443-62.
13. Le Jan, S., et al., *Functional overlap between chondroitin and heparan sulfate proteoglycans during VEGF-induced sprouting angiogenesis.* Arterioscler Thromb Vasc Biol, 2012. **32**(5): p. 1255-63.
14. Bode-Lesniewska, B., et al., *Distribution of the large aggregating proteoglycan versican in adult human tissues.* J Histochem Cytochem, 1996. **44**(4): p. 303-12.
15. Kimata, K., et al., *A large chondroitin sulfate proteoglycan (PG-M) synthesized before chondrogenesis in the limb bud of chick embryo.* J Biol Chem, 1986. **261**(29): p. 13517-25.
16. Shinomura, T., et al., *cDNA cloning of PG-M, a large chondroitin sulfate proteoglycan expressed during chondrogenesis in chick limb buds. Alternative spliced multiforms of PG-M and their relationships to versican.* J Biol Chem, 1993. **268**(19): p. 14461-9.
17. Zimmermann, D.R. and E. Ruoslahti, *Multiple domains of the large fibroblast proteoglycan, versican.* Embo J, 1989. **8**(10): p. 2975-81.
18. Wu, Y.J., et al., *The interaction of versican with its binding partners.* Cell Res, 2005. **15**(7): p. 483-94.
19. Zheng, P.S., et al., *Versican/PG-M G3 domain promotes tumor growth and angiogenesis.* FASEB J, 2004. **18**(6): p. 754-6.
20. Slevin, M., et al., *Hyaluronan-mediated angiogenesis in vascular disease: uncovering RHAMM and CD44 receptor signaling pathways.* Matrix Biol, 2007. **26**(1): p. 58-68.
21. Hattori, N., et al., *Pericellular versican regulates the fibroblast-myofibroblast transition: a role for ADAMTS5 protease-mediated proteolysis.* J Biol Chem, 2011. **286**(39): p. 34298-310.
22. Nandadasa, S., C.M. Nelson, and S.S. Apte, *ADAMTS9-Mediated Extracellular Matrix Dynamics Regulates Umbilical Cord Vascular Smooth Muscle Differentiation and Rotation.* Cell Rep, 2015. **11**(10): p. 1519-28.

23. Dours-Zimmermann, M.T. and D.R. Zimmermann, *A novel glycosaminoglycan attachment domain identified in two alternative splice variants of human versican.* J Biol Chem, 1994. **269**(52): p. 32992-8.
24. Mjaatvedt, C.H., et al., *The Cspg2 gene, disrupted in the hdf mutant, is required for right cardiac chamber and endocardial cushion formation.* Dev Biol, 1998. **202**(1): p. 56-66.
25. Yamamura, H., et al., *A heart segmental defect in the anterior-posterior axis of a transgenic mutant mouse.* Dev Biol, 1997. **186**(1): p. 58-72.
26. Camenisch, T.D., et al., *Disruption of hyaluronan synthase-2 abrogates normal cardiac morphogenesis and hyaluronan-mediated transformation of epithelium to mesenchyme.* J Clin Invest, 2000. **106**(3): p. 349-60.
27. Francis, S.E., et al., *Central roles of alpha5beta1 integrin and fibronectin in vascular development in mouse embryos and embryoid bodies.* Arterioscler Thromb Vasc Biol, 2002. **22**(6): p. 927-33.
28. Hunziker, E.B., W. Herrmann, and R.K. Schenk, *Ruthenium hexammine trichloride (RHT)-mediated interaction between plasmalemmal components and pericellular matrix proteoglycans is responsible for the preservation of chondrocytic plasma membranes in situ during cartilage fixation.* J Histochem Cytochem, 1983. **31**(6): p. 717-27.
29. Shalaby, F., et al., *A requirement for Flk1 in primitive and definitive hematopoiesis and vasculogenesis.* Cell, 1997. **89**(6): p. 981-90.
30. Ferkowicz, M.J., et al., *CD41 expression defines the onset of primitive and definitive hematopoiesis in the murine embryo.* Development, 2003. **130**(18): p. 4393-403.
31. Pijuan-Sala, B., et al., *A single-cell molecular map of mouse gastrulation and early organogenesis.* Nature, 2019. **566**(7745): p. 490-495.
32. Calabro, A., et al., *Microanalysis of enzyme digests of hyaluronan and chondroitin/dermatan sulfate by fluorophore-assisted carbohydrate electrophoresis (FACE).* Glycobiology, 2000. **10**(3): p. 273-81.
33. Calabro, A., V.C. Hascall, and R.J. Midura, *Adaptation of FACE methodology for microanalysis of total hyaluronan and chondroitin sulfate composition from cartilage.* Glycobiology, 2000. **10**(3): p. 283-93.
34. Midura, R.J., et al., *Quantification of hyaluronan (HA) using a simplified fluorophore-assisted carbohydrate electrophoresis (FACE) procedure.* Methods Cell Biol, 2018. **143**: p. 297-316.
35. De Angelis, J.E., et al., *Tmem2 Regulates Embryonic Vegf Signaling by Controlling Hyaluronic Acid Turnover.* Dev Cell, 2017. **40**(2): p. 123-136.
36. Schinzel, R.T., et al., *The Hyaluronidase, TMEM2, Promotes ER Homeostasis and Longevity Independent of the UPR(ER).* Cell, 2019. **179**(6): p. 1306-1318.e18.
37. Yamamoto, H., et al., *A mammalian homolog of the zebrafish transmembrane protein 2 (TMEM2) is the long-sought-after cell-surface hyaluronidase.* J Biol Chem, 2017. **292**(18): p. 7304-7313.
38. Bai, K.J., et al., *The role of hyaluronan synthase 3 in ventilator-induced lung injury.* Am J Respir Crit Care Med, 2005. **172**(1): p. 92-8.
39. Mack, J.A., et al., *Enhanced inflammation and accelerated wound closure following tetraphorbol ester application or full-thickness wounding in mice lacking hyaluronan synthases Has1 and Has3.* J Invest Dermatol, 2012. **132**(1): p. 198-207.
40. Doudna, J.A. and E. Charpentier, *Genome editing. The new frontier of genome engineering with CRISPR-Cas9.* Science, 2014. **346**(6213): p. 1258096.
41. Jinek, M., et al., *A programmable dual-RNA-guided DNA endonuclease in adaptive bacterial immunity.* Science, 2012. **337**(6096): p. 816-21.
42. Nagy, A., et al., *Derivation of completely cell culture-derived mice from early-passage embryonic stem cells.* Proc Natl Acad Sci U S A, 1993. **90**(18): p. 8424-8.

43. Baker, M., et al., *Use of the mouse aortic ring assay to study angiogenesis.* Nat Protoc, 2012. **7**(1): p. 89-104.
44. Wang, A. and V.C. Hascall, *Hyaluronan structures synthesized by rat mesangial cells in response to hyperglycemia induce monocyte adhesion.* J Biol Chem, 2004. **279**(11): p. 10279-85.
45. Selbi, W., et al., *Characterization of hyaluronan cable structure and function in renal proximal tubular epithelial cells.* Kidney Int, 2006. **70**(7): p. 1287-95.
46. Gueye, N.A., et al., *Versican Proteolysis by ADAMTS Proteases and Its Influence on Sex Steroid Receptor Expression in Uterine Leiomyoma.* J Clin Endocrinol Metab, 2017. **102**(5): p. 1631-1641.
47. Keire, P.A., et al., *Inhibition of versican expression by siRNA facilitates tropoelastin synthesis and elastic fiber formation by human SK-LMS-1 leiomyosarcoma smooth muscle cells in vitro and in vivo.* Matrix Biol, 2016. **50**: p. 67-81.
48. Buschmann, M.D. and A.J. Grodzinsky, *A molecular model of proteoglycan-associated electrostatic forces in cartilage mechanics.* J Biomech Eng, 1995. **117**(2): p. 179-92.
49. Szabo, A., et al., *In vivo confinement promotes collective migration of neural crest cells.* J Cell Biol, 2016. **213**(5): p. 543-55.
50. Shukla, S., et al., *Synthesis and organization of hyaluronan and versican by embryonic stem cells undergoing embryoid body differentiation.* J Histochem Cytochem, 2010. **58**(4): p. 345-58.
51. Chan, C.K., et al., *Differentiation of cardiomyocytes from human embryonic stem cells is accompanied by changes in the extracellular matrix production of versican and hyaluronan.* J Cell Biochem, 2010. **111**(3): p. 585-96.
52. Evanko, S.P., et al., *Hyaluronan-dependent pericellular matrix.* Adv Drug Deliv Rev, 2007. **59**(13): p. 1351-65.
53. Protin, U., et al., *CD44-deficient mice develop normally with changes in subpopulations and recirculation of lymphocyte subsets.* J Immunol, 1999. **163**(9): p. 4917-23.
54. Evanko, S.P., J.C. Angello, and T.N. Wight, *Formation of hyaluronan- and versican-rich pericellular matrix is required for proliferation and migration of vascular smooth muscle cells.* Arterioscler Thromb Vasc Biol, 1999. **19**(4): p. 1004-13.
55. George, E.L., et al., *Defects in mesoderm, neural tube and vascular development in mouse embryos lacking fibronectin.* Development, 1993. **119**(4): p. 1079-91.
56. Suwan, K., et al., *Versican/PG-M Assembles Hyaluronan into Extracellular Matrix and Inhibits CD44-mediated Signaling toward Premature Senescence in Embryonic Fibroblasts.* J Biol Chem, 2009. **284**(13): p. 8596-604.
57. Kloeckener-Gruissem, B., et al., *Identification of the genetic defect in the original Wagner syndrome family.* Mol Vis, 2006. **12**: p. 350-5.
58. Kloeckener-Gruissem, B., et al., *Novel VCAN mutations and evidence for unbalanced alternative splicing in the pathogenesis of Wagner syndrome.* Eur J Hum Genet, 2013. **21**(3): p. 352-6.
59. Rothschild, P.R., et al., *De novo splice mutation in the versican gene in a family with Wagner syndrome.* JAMA Ophthalmol, 2013. **131**(6): p. 805-7.
60. Burns, T.A., et al., *Imbalanced expression of Vcan mRNA splice form proteins alters heart morphology and cellular protein profiles.* PLoS One, 2014. **9**(2): p. e89133.
61. Dours-Zimmermann, M.T., et al., *Versican V2 assembles the extracellular matrix surrounding the nodes of ranvier in the CNS.* J Neurosci, 2009. **29**(24): p. 7731-42.
62. Nandadasa, S., S. Foulcer, and S.S. Apte, *The multiple, complex roles of versican and its proteolytic turnover by ADAMTS proteases during embryogenesis.* Matrix Biol, 2014. **35**: p. 34-41.
63. Nandadasa, S., et al., *Vascular dimorphism ensured by regulated proteoglycan dynamics favors rapid umbilical artery closure at birth.* bioRxiv, 2020: p. 2020.07.02.184978.

64. Hope, C., et al., *Immunoregulatory roles of versican proteolysis in the myeloma microenvironment.* Blood, 2016. **128**(5): p. 680-5.
65. McCulloch, D.R., et al., *ADAMTS metalloproteases generate active versican fragments that regulate interdigital web regression.* Dev Cell, 2009. **17**(5): p. 687-98.
66. Islam, S., et al., *Accumulation of versican facilitates wound healing: implication of its initial ADAMTS-cleavage site.* Matrix Biol, 2019.
67. Fidler, A.L., et al., *Collagen IV and basement membrane at the evolutionary dawn of metazoan tissues.* Elife, 2017. **6**.
68. Miner, J.H., et al., *Compositional and structural requirements for laminin and basement membranes during mouse embryo implantation and gastrulation.* Development, 2004. **131**(10): p. 2247-56.
69. Rodin, S., et al., *Long-term self-renewal of human pluripotent stem cells on human recombinant laminin-511.* Nat Biotechnol, 2010. **28**(6): p. 611-5.
70. Asano, K., et al., *Stromal Versican Regulates Tumor Growth by Promoting Angiogenesis.* Sci Rep, 2017. **7**(1): p. 17225.
71. Oladipupo, S.S., et al., *Impaired tumor growth and angiogenesis in mice heterozygous for Vegfr2 (Flk1).* Sci Rep, 2018. **8**(1): p. 14724.
72. Zhao, Y. and R.P. Singh, *The role of anti-vascular endothelial growth factor (anti-VEGF) in the management of proliferative diabetic retinopathy.* Drugs Context, 2018. **7**: p. 212532.
73. Arranz, A.M., et al., *Hyaluronan deficiency due to Has3 knock-out causes altered neuronal activity and seizures via reduction in brain extracellular space.* J Neurosci, 2014. **34**(18): p. 6164-76.
74. Matsumoto, K., et al., *Conditional inactivation of Has2 reveals a crucial role for hyaluronan in skeletal growth, patterning, chondrocyte maturation and joint formation in the developing limb.* Development, 2009. **136**(16): p. 2825-35.
75. Tallquist, M.D. and P. Soriano, *Epiblast-restricted Cre expression in MORE mice: a tool to distinguish embryonic vs. extra-embryonic gene function.* Genesis, 2000. **26**(2): p. 113-5.

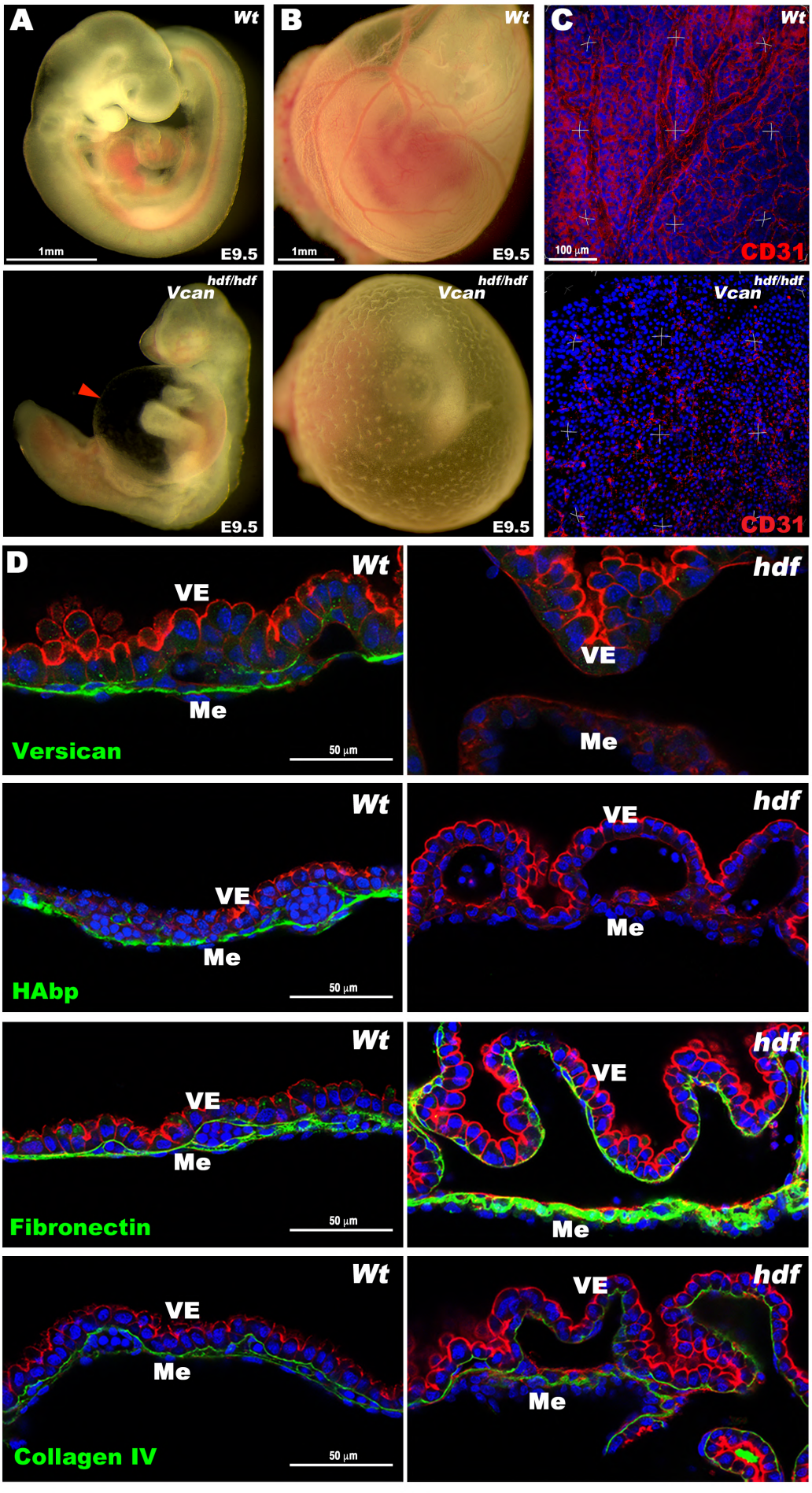
A
Wt
1mm
E9.5
B
Wt
1mm
E9.5
C
Wt
100 μm
CD31
hdf/hdf
Vcan
E9.5
hdf/hdf
Vcan
E9.5
hdf/hdf
Vcan
CD31
D
Wt
VE
Me
Versican
50 μm
hdf
VE
Me
Wt
VE
Me
HAbp
50 μm
hdf
VE
Me
Wt
VE
Me
Fibronectin
50 μm
hdf
VE
Me
Wt
VE
Me
Collagen IV
50 μm
hdf
VE
Me

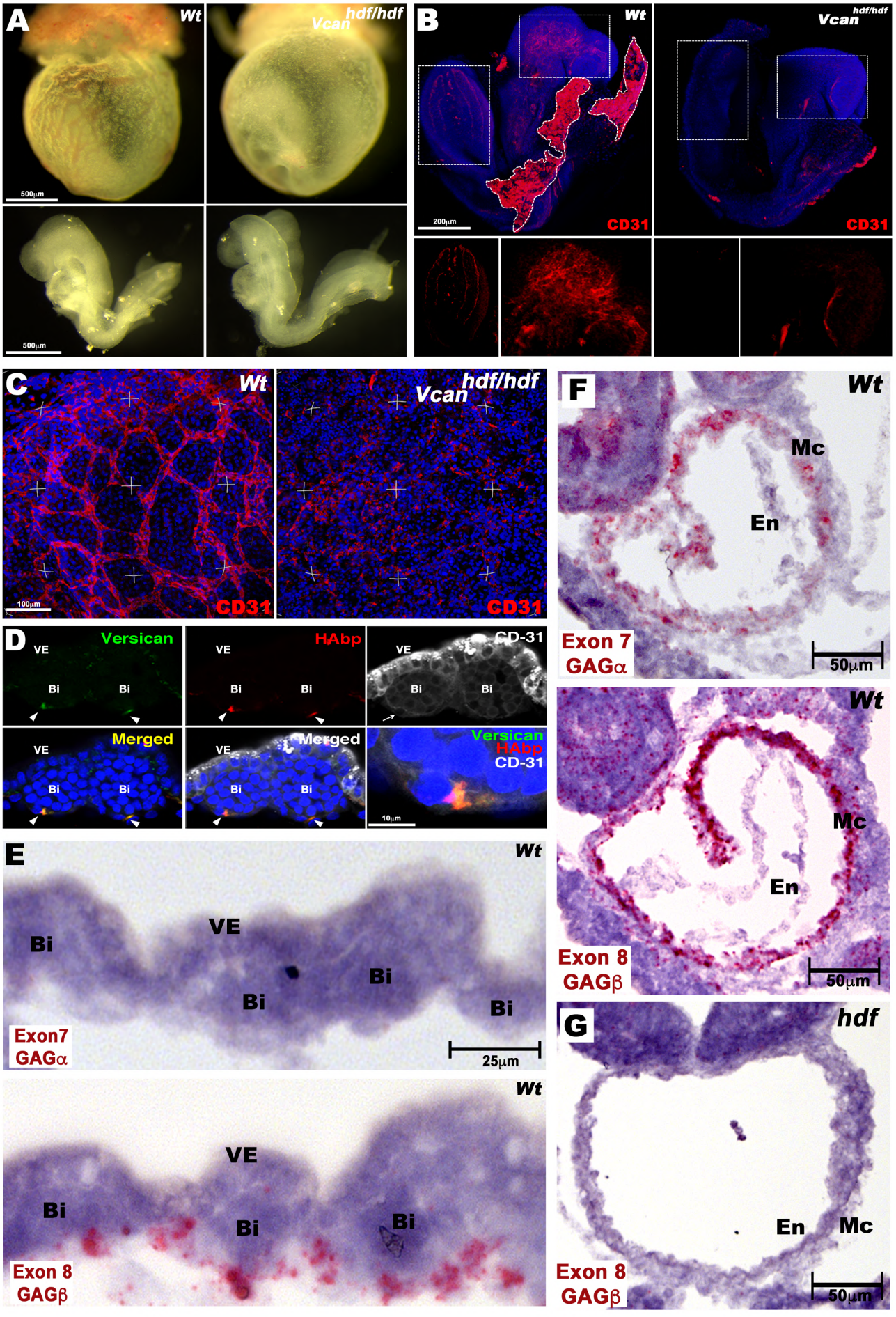
A
Wt
Vcan hdf/hdf
500μm
500μm
B
Wt
Vcan hdf/hdf
200μm
CD31
CD31
C
Wt
Vcan hdf/hdf
100μm
CD31
CD31
D
Versican
HAbp
CD-31
Merged
Merged
Versican
HAbp
CD-31
VE
Bi
10μm
E
Wt
VE
Bi
Exon7
GAGα
25μm
Wt
VE
Bi
Exon 8
GAGβ
F
Wt
Mc
En
Exon 7
GAGα
50μm
Wt
Mc
En
Exon 8
GAGβ
50μm
G
hdf
En
Mc
Exon 8
GAGβ
50μm

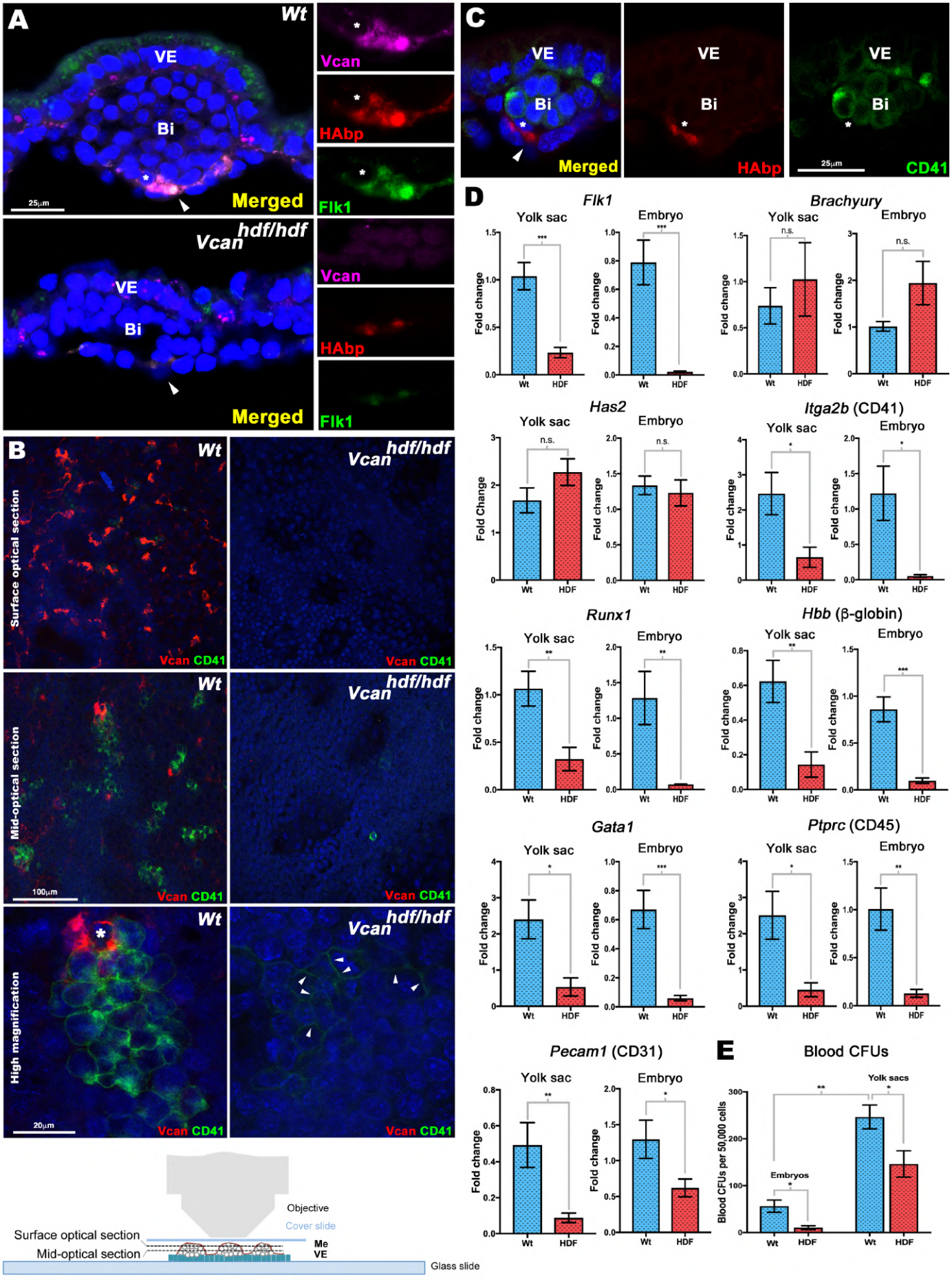
A
Wt
VE
Bi
Merged
Vcan
HAbp
Flk1
Vcan hdf/hdf
B
Surface optical section
Mid-optical section
High magnification
Vcan CD41
100µm
20µm
C
CD41
25µm
D
Flk1
Brachyury
Has2
Itga2b (CD41)
Runx1
Hbb (β-globin)
Gata1
Ptprc (CD45)
Pecam1 (CD31)
Yolk sac
Embryo
Fold change
n.s.
Wt
HDF
E
Blood CFUs
Yolk sacs
Embryos
Blood CFUs per 50,000 cells
Objective
Cover slide
Me
Glass slide

Figure-4

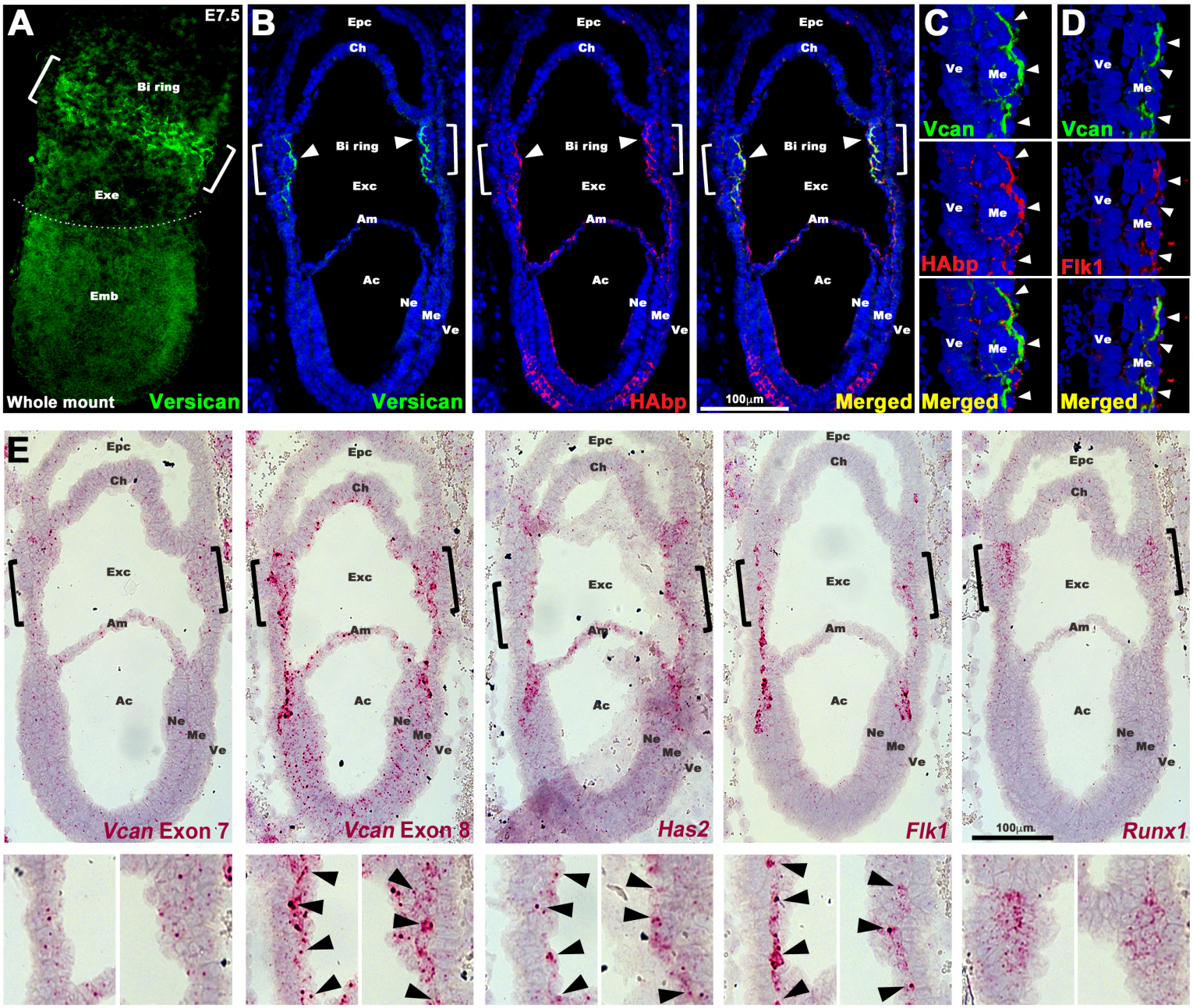
A
E7.5
Bi ring
Exe
Emb
Whole mount
Versican
B
Epc
Ch
Bi ring
Exc
Am
Ac
Ne
Me
Ve
Versican
HAbp
100μm
Merged
C
Vcan
HAbp
Merged
D
Vcan
Flk1
Merged
E
Vcan Exon 7
Vcan Exon 8
Has2
Flk1
Runx1

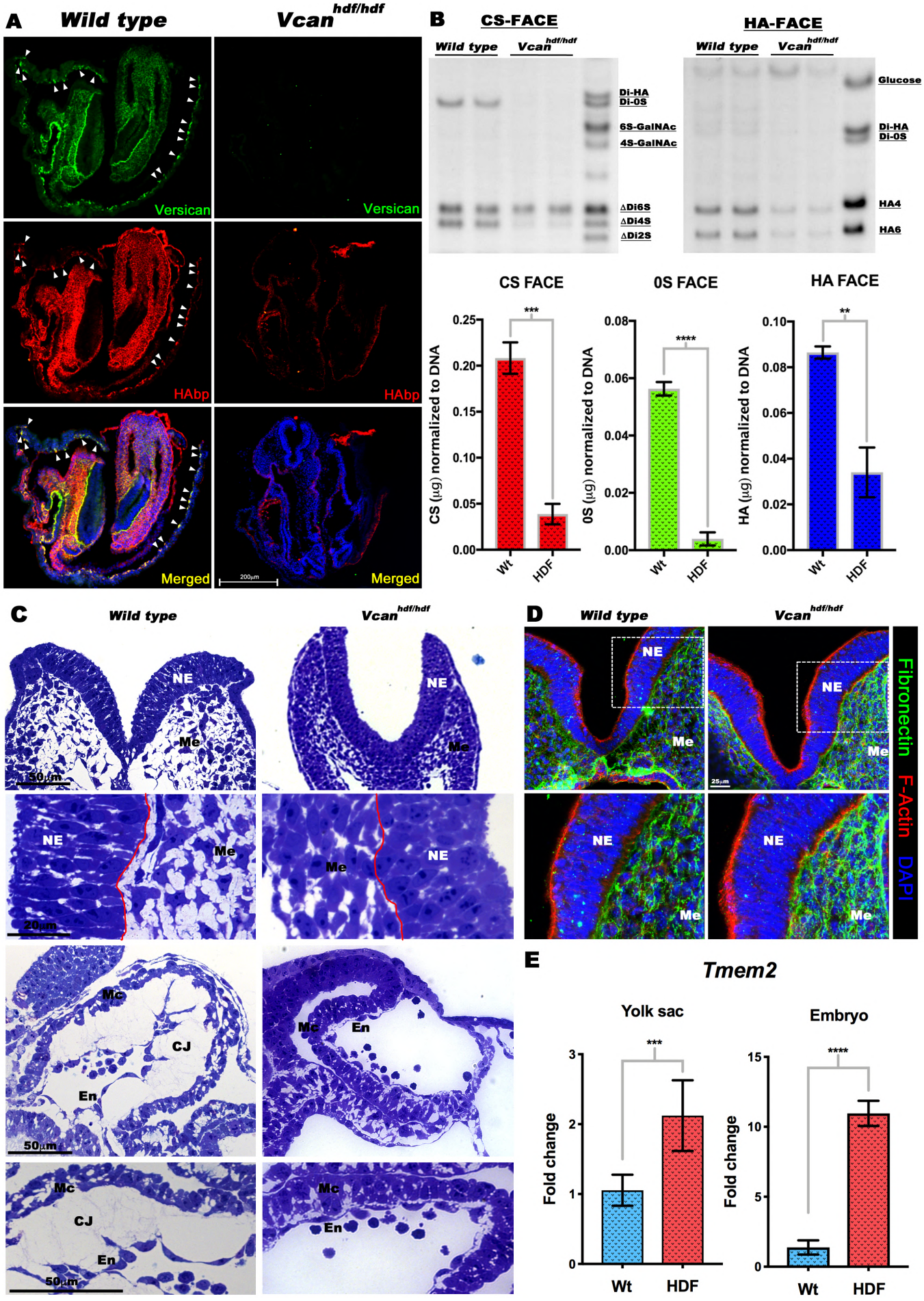
A
Wild type
Vcan hdf/hdf
Versican
Versican
HAbp
HAbp
Merged
Merged
200µm
B
CS-FACE
HA-FACE
Wild type
Vcan hdf/hdf
Wild type
Vcan hdf/hdf
Di-HA
Di-0S
6S-GalNAc
4S-GalNAc
ΔDi6S
ΔDi4S
ΔDi2S
Glucose
Di-HA
Di-0S
HA4
HA6
CS FACE
0S FACE
HA FACE
CS (µg) normalized to DNA
0S (µg) normalized to DNA
HA (µg) normalized to DNA
***
****
**
Wt
HDF
C
Wild type
Vcan hdf/hdf
NE
Me
50µm
20µm
Mc
CJ
En
50µm
D
Wild type
Vcan hdf/hdf
NE
Me
25µm
Fibronectin
F-Actin
DAPI
E
Tmem2
Yolk sac
Embryo
Fold change
***
****
Wt
HDF

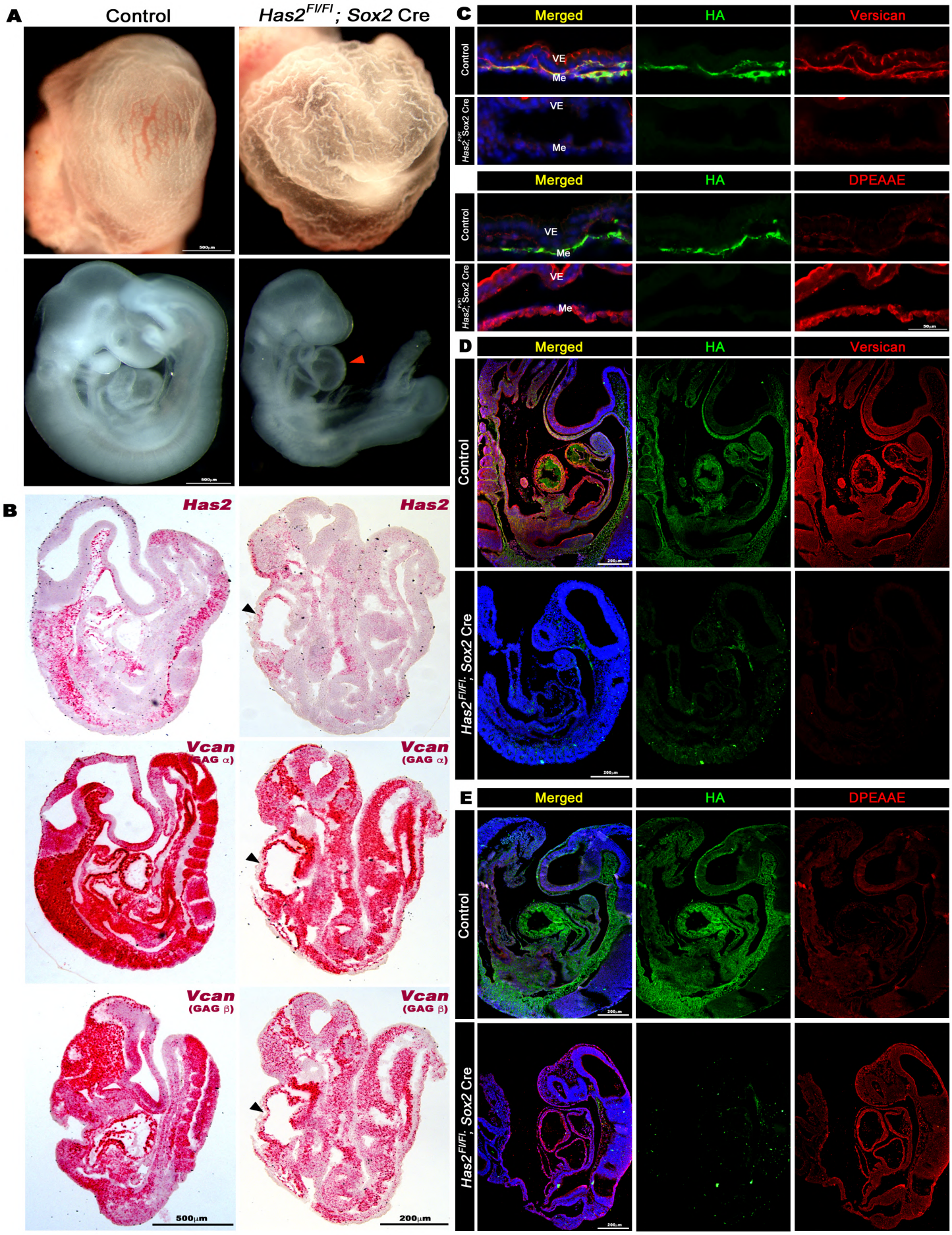
A
Control
Has2Fl/Fl; Sox2 Cre
B
Has2
Has2
Vcan (GAG α)
Vcan (GAG α)
Vcan (GAG β)
Vcan (GAG β)
500μm
200μm
C
Merged
HA
Versican
Control
VE
Me
Has2Fl/Fl; Sox2 Cre
Merged
HA
DPEAAE
Control
VE
Me
Has2Fl/Fl; Sox2 Cre
D
Merged
HA
Versican
Control
Has2Fl/Fl; Sox2 Cre
E
Merged
HA
DPEAAE
Control
Has2Fl/Fl; Sox2 Cre

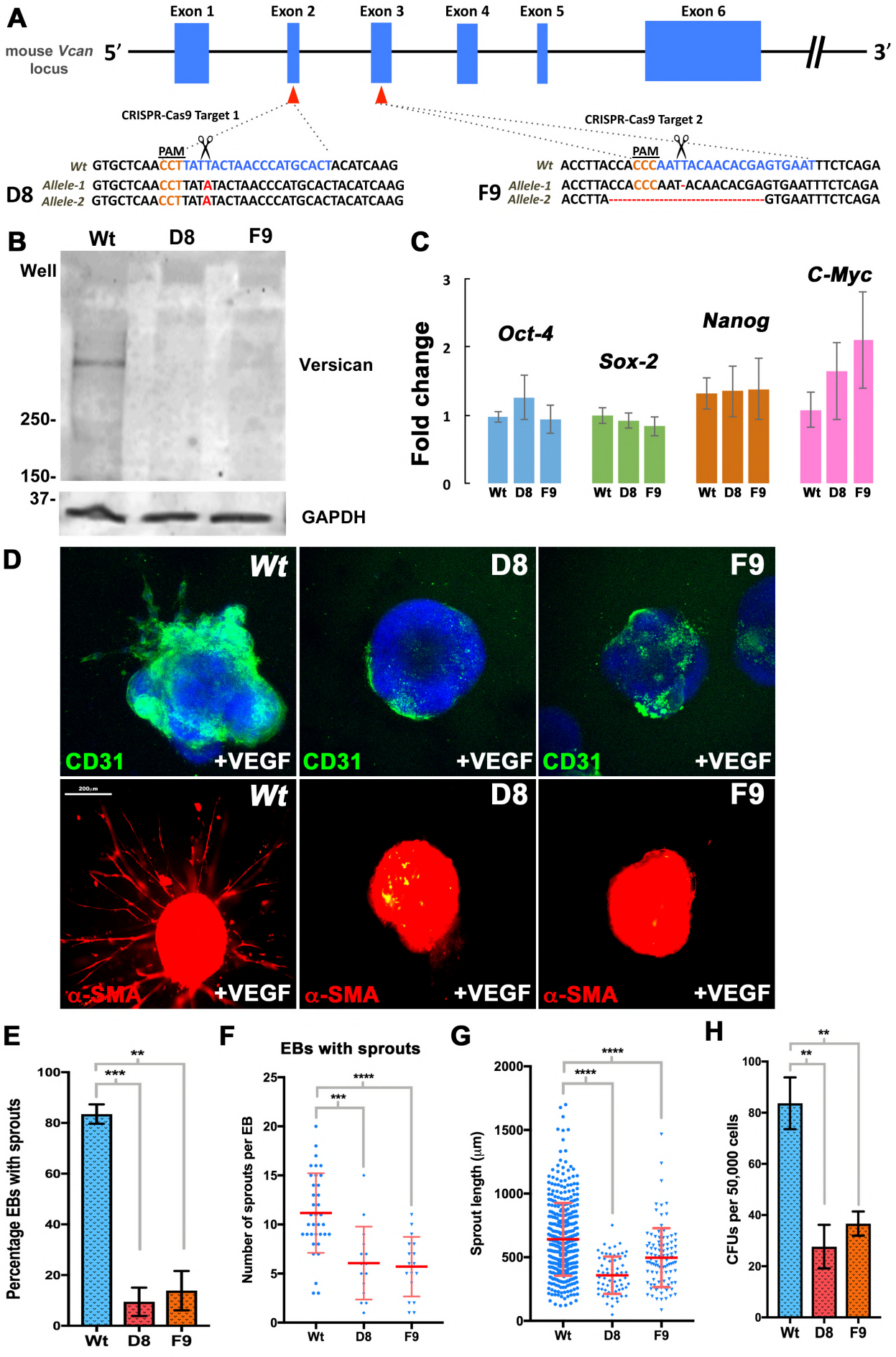
A
mouse Vcan locus
5′
3′
Exon 1
Exon 2
Exon 3
Exon 4
Exon 5
Exon 6
CRISPR-Cas9 Target 1
CRISPR-Cas9 Target 2
PAM
Wt GTGCTCAACCTTATTACTAACCCATGCACTACATCAAG
D8 Allele-1 GTGCTCAACCTTATATACTAACCCATGCACTACATCAAG
Allele-2 GTGCTCAACCTTATATACTAACCCATGCACTACATCAAG
Wt ACCTTACCACCCAATTACAACACGAGTGAATTTCTCAGA
F9 Allele-1 ACCTTACCACCCAAT-ACAACACGAGTGAATTTCTCAGA
Allele-2 ACCTTA----------GTGAATTTCTCAGA
B
Wt
D8
F9
Well
250-
150-
37-
Versican
GAPDH
C
Fold change
Oct-4
Sox-2
Nanog
C-Myc
Wt D8 F9
D
Wt
D8
F9
CD31
+VEGF
α-SMA
+VEGF
E
Percentage EBs with sprouts
F
EBs with sprouts
Number of sprouts per EB
G
Sprout length (μm)
H
CFUs per 50,000 cells
Wt
D8
F9

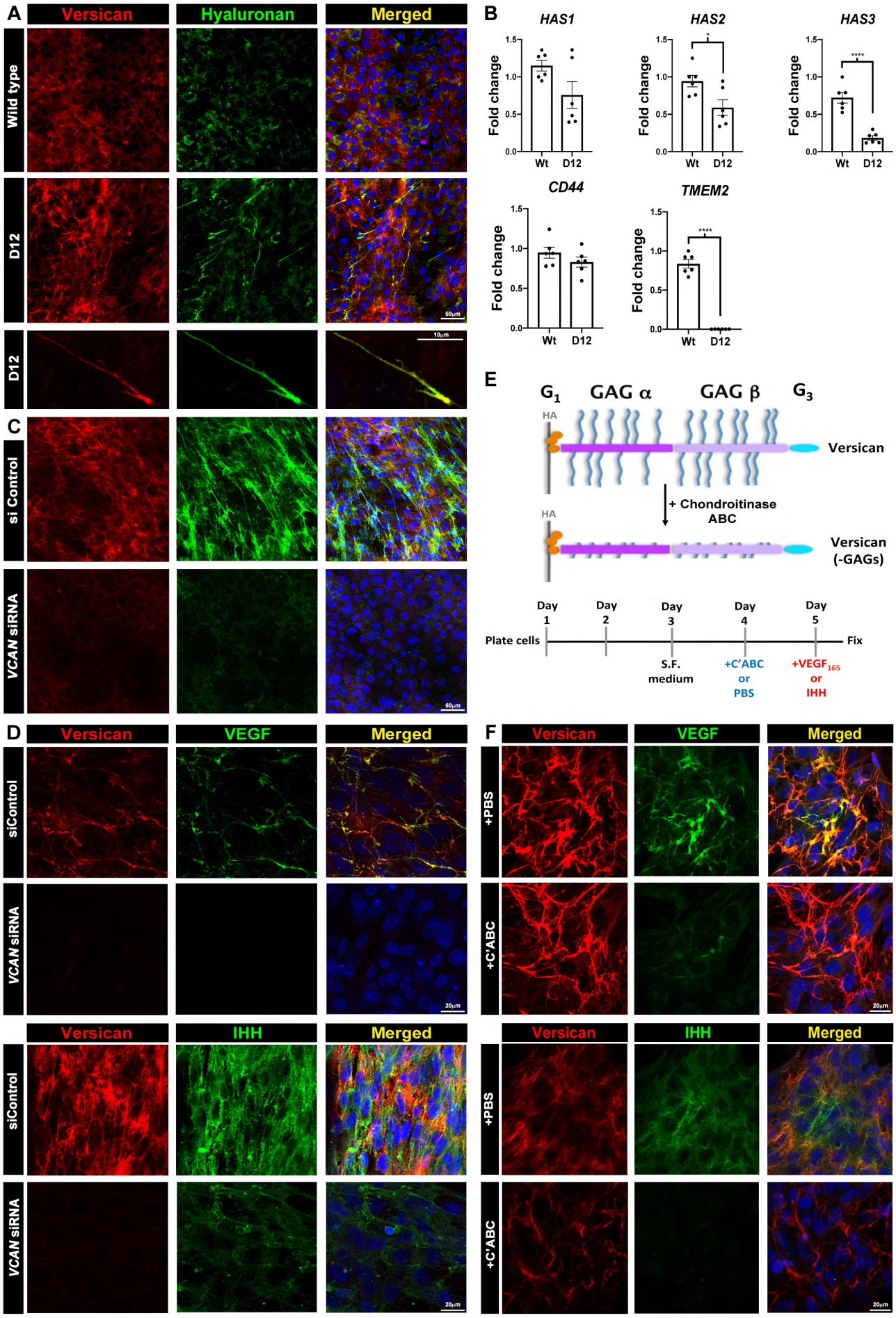
A
Versican
Hyaluronan
Merged
Wild type
D12
D12
50µm
10µm
C
si Control
VCAN siRNA
50µm
B
HAS1
HAS2
HAS3
CD44
TMEM2
Fold change
Wt
D12
E
G1
GAG α
GAG β
G3
HA
Versican
+ Chondroitinase ABC
Versican (-GAGs)
Day 1
Day 2
Day 3
Day 4
Day 5
Plate cells
Fix
S.F. medium
+C'ABC or PBS
+VEGF165 or IHH
D
Versican
VEGF
Merged
siControl
VCAN siRNA
20µm
IHH
F
+PBS
+C'ABC

Figure-9

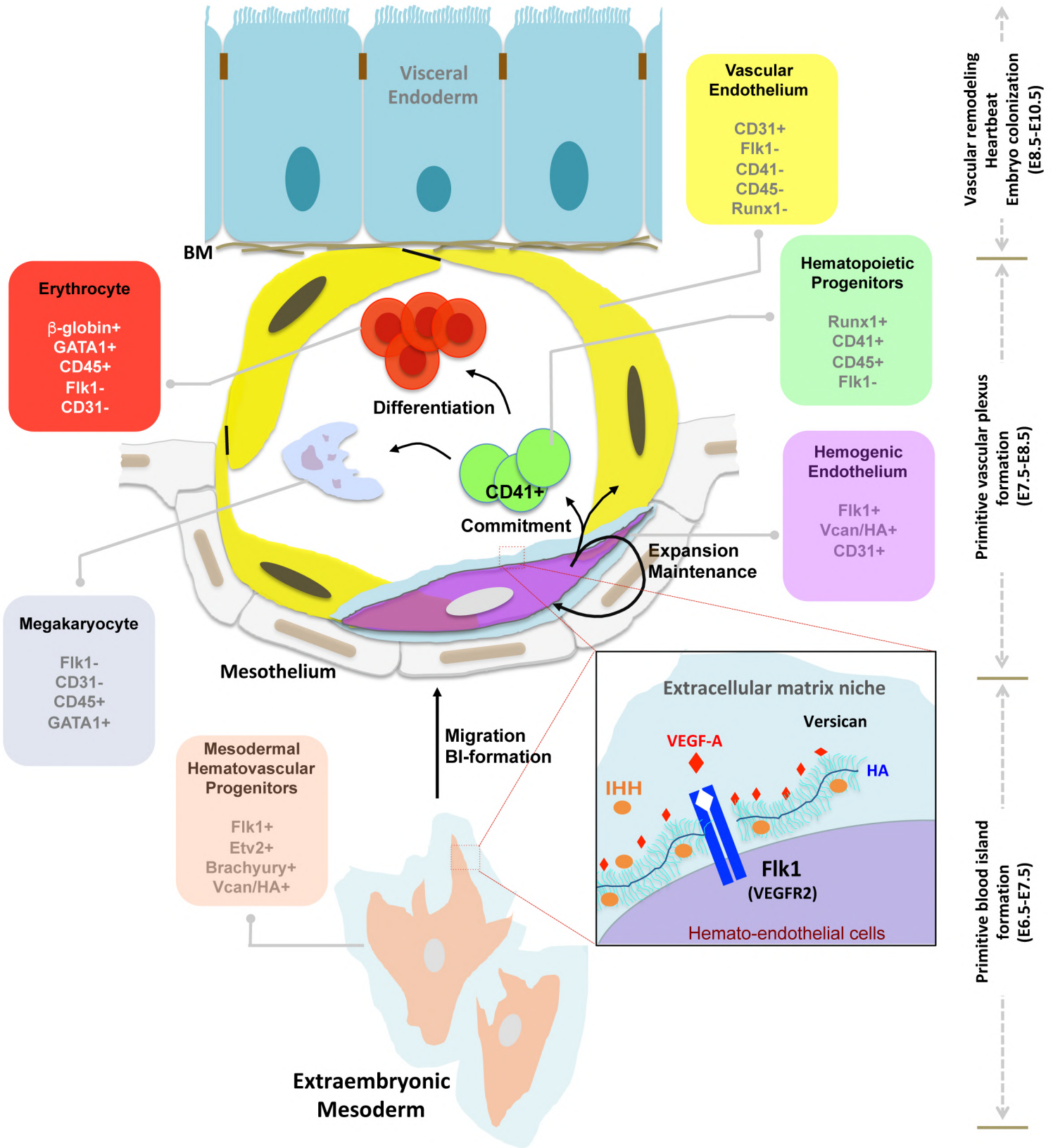
Visceral Endoderm
BM
Vascular Endothelium
CD31+
Flk1-
CD41-
CD45-
Runx1-
Erythrocyte
β-globin+
GATA1+
CD45+
Flk1-
CD31-
Hematopoietic Progenitors
Runx1+
CD41+
CD45+
Flk1-
Differentiation
CD41+
Commitment
Expansion
Maintenance
Hemogenic Endothelium
Flk1+
Vcan/HA+
CD31+
Megakaryocyte
Flk1-
CD31-
CD45+
GATA1+
Mesothelium
Migration
BI-formation
Mesodermal Hematovascular Progenitors
Flk1+
Etv2+
Brachyury+
Vcan/HA+
Extracellular matrix niche
Versican
VEGF-A
HA
IHH
Flk1
(VEGFR2)
Hemato-endothelial cells
Extraembryonic Mesoderm
Vascular remodeling
Heartbeat
Embryo colonization
(E8.5-E10.5)
Primitive vascular plexus formation
(E7.5-E8.5)
Primitive blood island formation
(E6.5-E7.5)

The versican-hyaluronan complex provides an essential extracellular matrix niche for Flk1^{+} hematoendothelial progenitors

Sumeda Nandadasa, Anna O'Donnell, Ayako Murao, Yu Yamaguchi, PhD, Ronald J. Midura, Lorin Olson and Suneel S. Apte

SUPPLEMENTAL FIGURES AND TABLE

Supplemental Figure 1

A

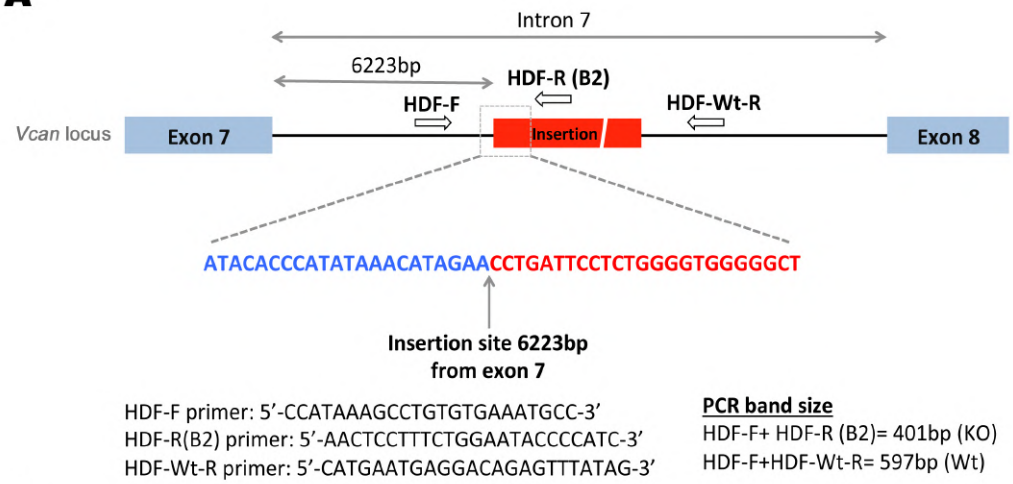

B

HDF-F primer ⇨

CCATAAAGCCTGTGTGAAATGCCATTAAAAAAATCCATTAACCATG
GTACTAGTATATTCAAGTCAAGCTGTTAAAATACACCCATATAAACA
TAGAACCTGATTCCTCTGGGGTGGGGGCTGGGAAAGAATCTGAGC
TGTTAGGAATAAGAAATCCCAAGGTTTCCAGAAGTCTGGTAAGTAG
CCGTCTGGGGGTGGTGATGGTGGTGGTGGTGGTGGTGGTGG
GGCGAGCTGATCTGCACCCCCCTGCCCACTAGGAAGCGGTCGTCGC
CGCCGCAGCTGTTGGCACTGACCGCGCAGGATTGGAAAGTTGTAAT
CCCATGGTCAGAGGGGTAAGCTCGCGCCGAGCAGGTCCCAGAGTC
GCCACTGCCAAG**GATGGGGTATTCCAGAAAGGAGTT**

⇦ **HDF-R (B2) primer**

Supplemental Figure 1: Characterization of the *Vcan*^{hdf} mutation and genotyping strategy.
(A) *Vcan*^{hdf} locus, showing the insertion site of the *Hoxa1-lacZ* transgene in intron 7. *Vcan* exons are indicated in blue and the insertion in red. Primer sequences and amplicons used for genotyping are shown at the bottom. **(B)** Sequence of the 401bp *Vcan*^{hdf} amplicon and the primer sequences used (underlined). The *Vcan* intron 7 sequence is in blue text and sequence corresponding to the *Hoxa1-lacZ* transgene is in red text.

Supplemental Figure 2

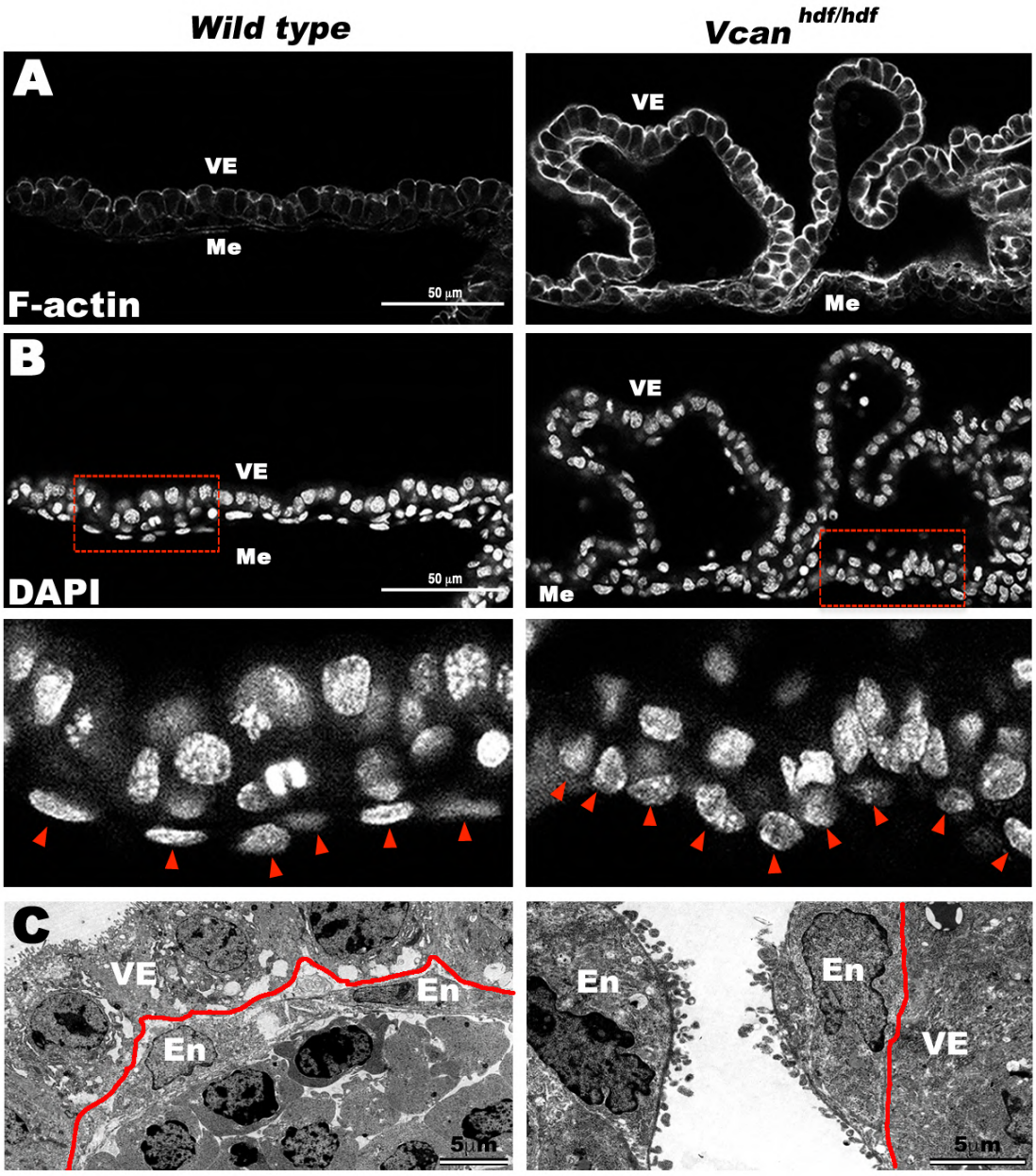

Supplemental Figure 2: Severe disorganization and cellular changes in *Vcan*$^{hdf/hdf}$ yolk sacs
(A) E9.5 *Vcan*$^{hdf/hdf}$ yolk sacs show dramatically increased F-actin staining.
(B) DAPI staining shows altered nuclear morphology and disrupted cellular organization of the *Vcan*$^{hdf/hdf}$ yolk sac mesoderm (Me) and mesothelium and (with **A**) separation from visceral endoderm (VE). Higher magnifications of the boxed areas (red line) in the upper panels of **B** are shown below. Arrowheads identify the nuclei of yolk sac mesothelium, which are rounded in *Vcan*$^{hdf/hdf}$ yolk sac.
(C) Transmission electron microscopy (TEM) images of wild type and *Vcan*$^{hdf/hdf}$ yolk sacs showing endothelium-lined blood islands in the wild type and detached vascular endothelial cells in the *Vcan*$^{hdf/hdf}$ yolk sac. The red line marks the basement membrane of the visceral endoderm, En=vascular endothelium. Scale bars in **A-B**= 50μm, 5μm in **C**.

Supplemental Figure 3

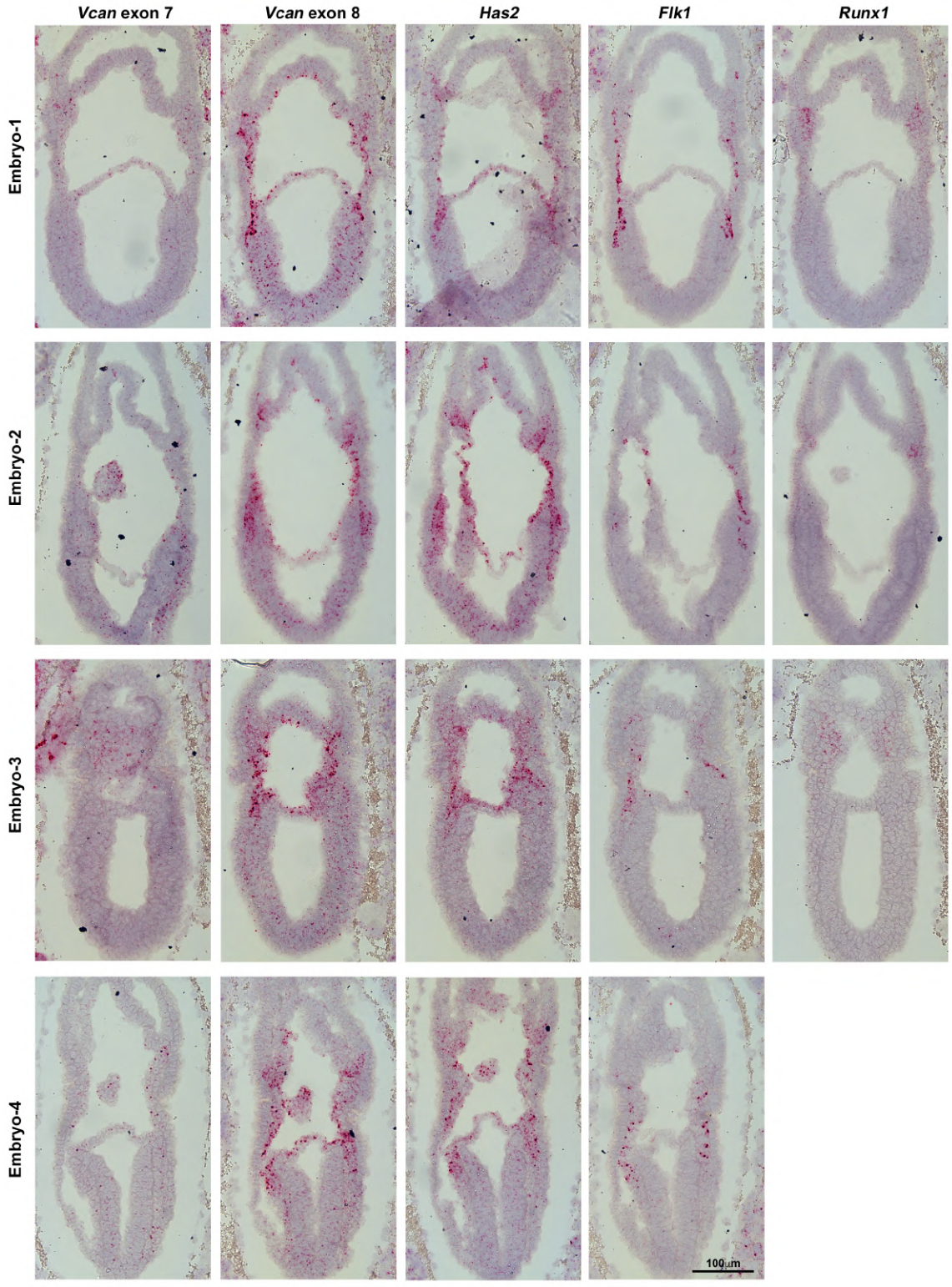

Supplemental Figure 3: RNAScope *in situ* hybridization of *Vcan* exon 7, *Vcan* exon 8, *Has2*, *Flk1* and *Runx1* probes to consecutive sections from four individual E7.5 wild type embryos. Hybridization signal is red, sections were counterstained with hematoxylin (blue). Scale bar = 100μm.

Supplemental Figure 4

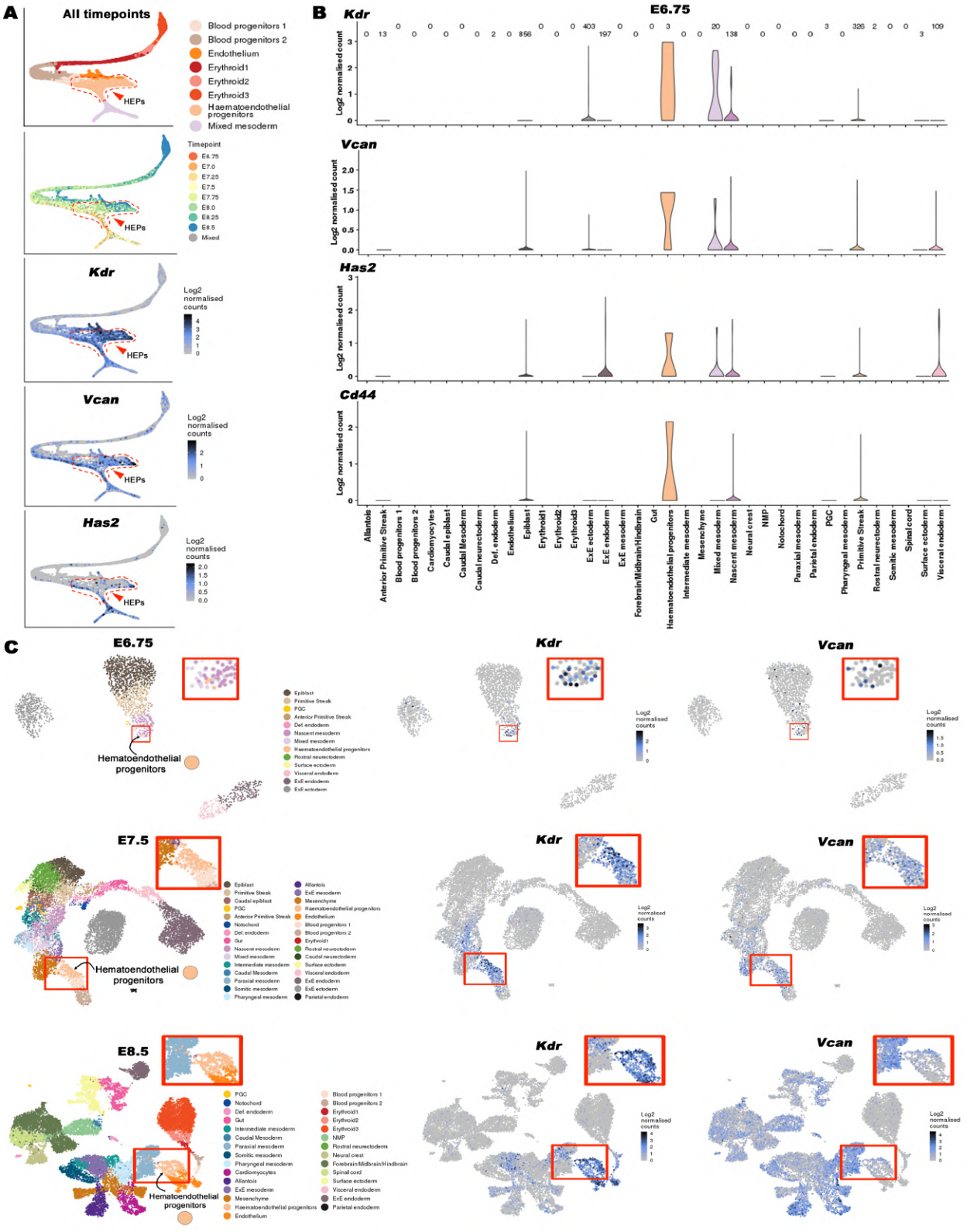

Supplemental Figure 4: Data extracted from a published single cell transcriptome atlas of mouse gastrulation illustrates specific *Vcan* and *Has2* expression by *Kdr*-expressing hematoendothelial cells.
(A) Force-directed graph layout of blood-related lineages showing the lineage-specific and time-resolved expression of *Kdr, Vcan* and *Has2*. The stippled red line encircles hematoendothelial progenitors.
(B) Violin plots of *Kdr, Vcan*, *Has2* and *Cd44* expression by cells of various lineages from E6.75 embryos. Note strong co-expression of these genes by single hematoendothelial progenitors.
(C) Uniform manifold approximation and projection (UMAP) plots showing overlap between single cell *Kdr* and *Vcan* expression at different gestational ages. High magnification inserts of hematoendothelial progenitors are indicated within red boxes.

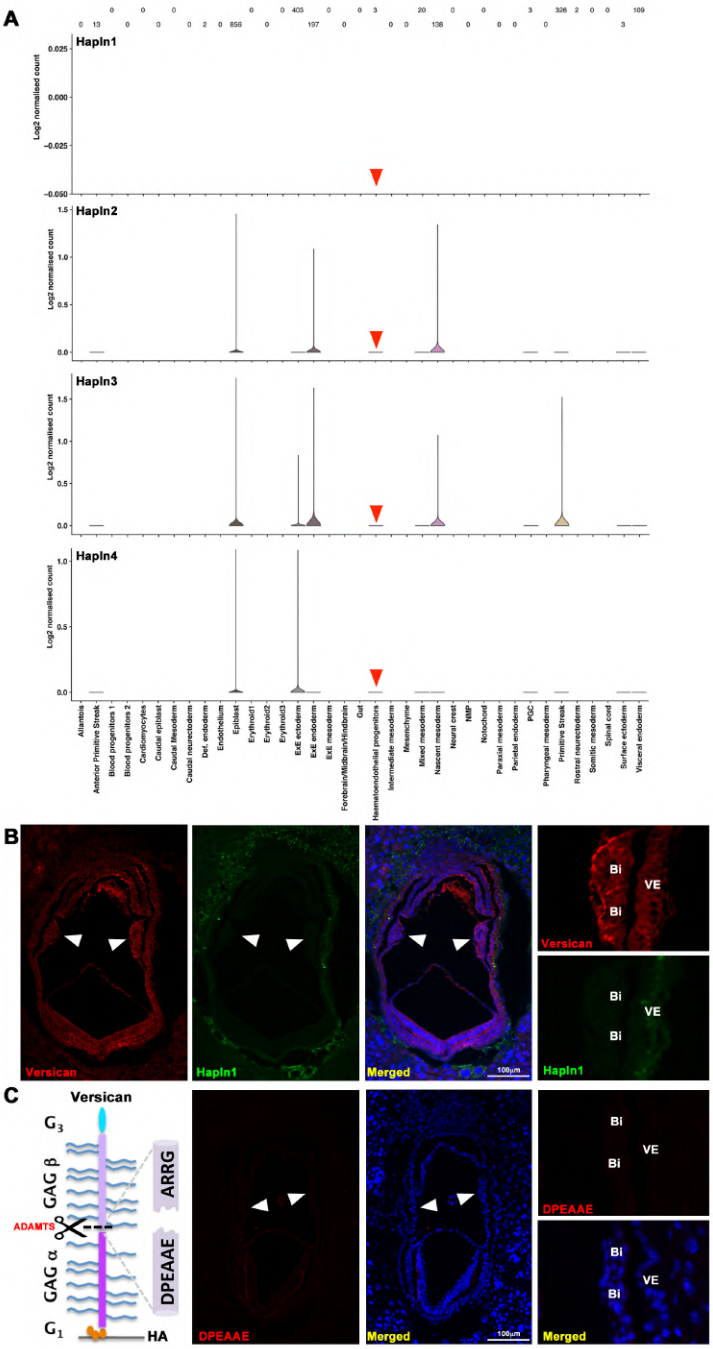

Supplemental Figure 5

Supplemental Figure 5: Data extracted from a published single cell transcriptome atlas of mouse gastrulation illustrates lack of link protein gene expression by hematoendothelial progenitors and versican cleavage in blood islands.
(A) Violin plots for *Hapln1-4* expression by cells of various lineages from E6.75 embryos. No expression of *Hapln1-4* is detected in hematoendothelial progenitors (red arrowhead) at this stage.
(B) HAPLN1 staining was not detected in E7.5 blood islands marked by versican staining (white arrowheads).
(C) ADAMTS-cleaved versican staining (anti-DPEAAE) is undetectable in E7.5 blood islands (white arrowheads). Scale bars = 100μm in **B** and **C**.

Supplemental Figure 6

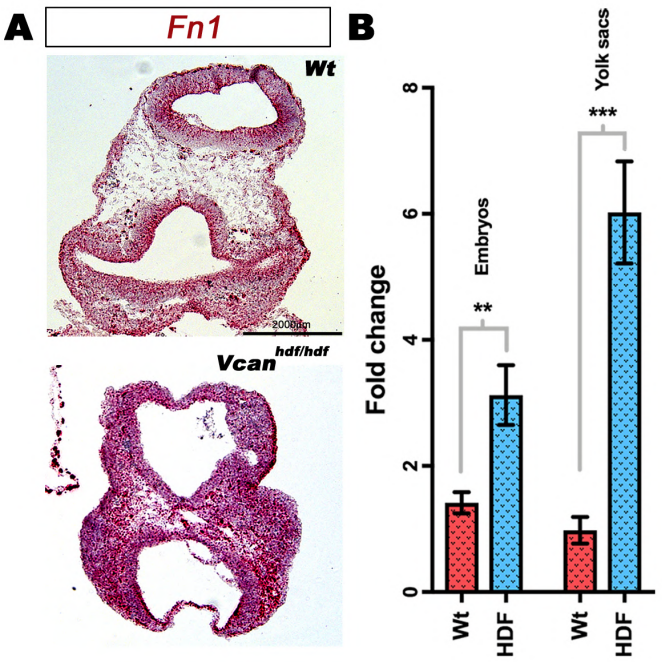

Supplemental Figure 6: Increased *Fn1* transcription in *Vcan*$^{hdf/hdf}$ embryos
(A) RNAscope *in-situ* hybridization of E9.5 wild type and *Vcan*$^{hdf/hdf}$ embryos showing stronger *Fn1* RNA expression in the mutant embryo.
(B) RT-qPCR analysis of *Fn1* transcript in wild type and *Vcan*$^{hdf/hdf}$ embryos and yolk sacs showing significantly increased expression in the mutant. (n=3 embryos and yolk sacs each genotype, error bars= S.E.M., **, p<0.01; ***, p<0.0001). Scale bars = 100μm in **A**.

Supplemental Figure 7

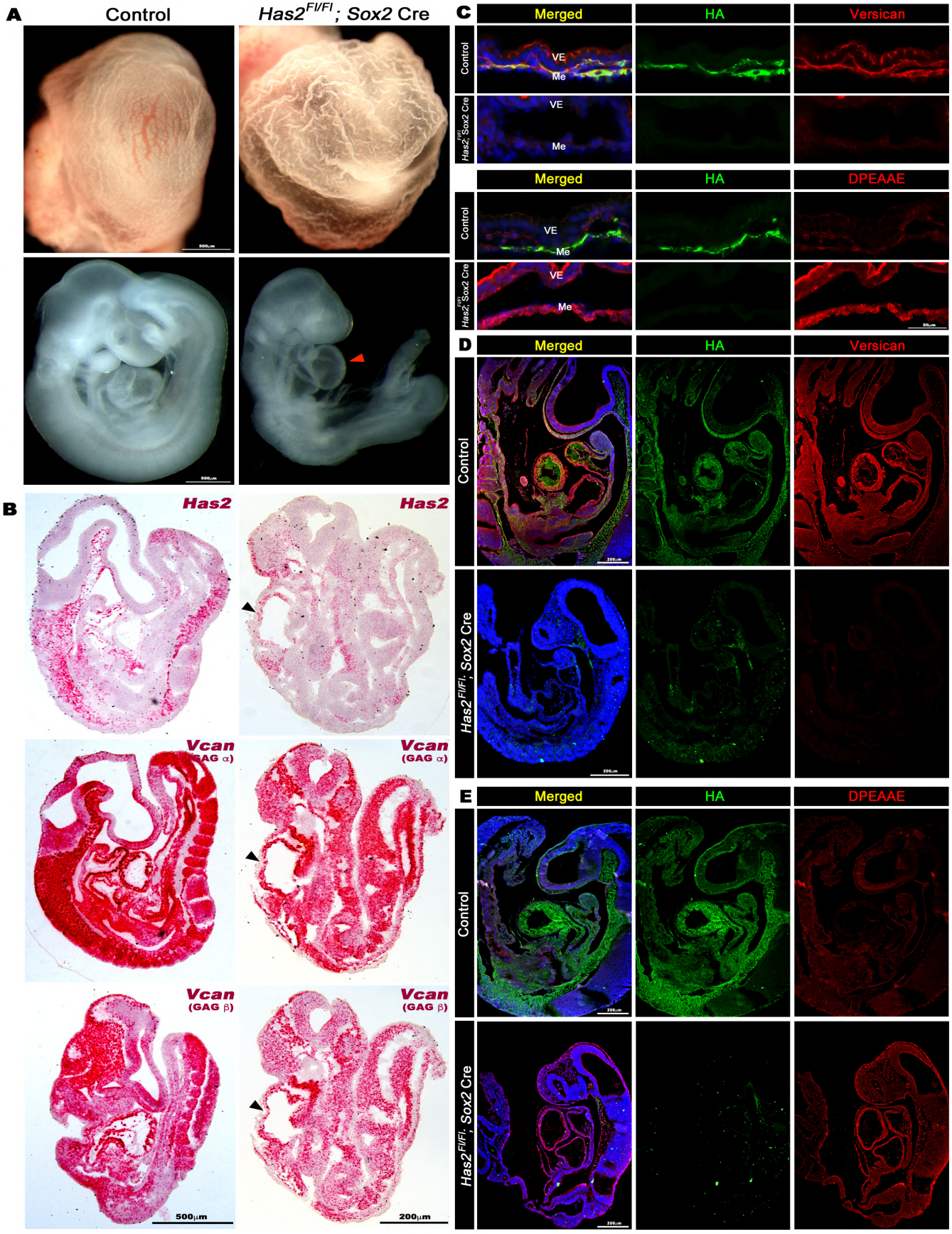

Supplemental Figure 7: Loss of yolk sac vasculature, HA and versican staining in *Has2* conditionally deleted embryos

(A) Whole mount images of *Has2*$^{Fl/Fl}$*; Sox2*Cre yolk sacs and embryos showing loss of yolk sac vasculature and a heart defect (red arrowhead indicates the enlarged heart) compared to control littermates (N=8 each genotype).

(B) RNAScope in situ hybridization for *Has2, Vcan* exon 7 (GAG α) and *Vcan* exon 8 (GAG β) shows residual *Has2* transcript and slightly reduced *Vcan* transcript in *Has2*$^{Fl/Fl}$*; Sox2* Cre embryos (n=4 embryos each probe).

(C) *Has2*$^{Fl/Fl}$*; Sox2* Cre yolk sacs show loss of HA and versican staining (upper panels) and increased versican catabolism is revealed by DPEAAE staining (lower panels) (N=4 each group).

(D) *Has2*$^{Fl/Fl}$*; Sox2* Cre embryos show loss of HA and versican staining (N=3 each group).

(E) *Has2*$^{Fl/Fl}$*; Sox2* Cre embryos show increased DPEAAE staining (N=3 each group).

Scale bars = 500μm in **A,B**; 50μm in in **C;** 200μm in **D**,**E**.

Supplemental Figure 8

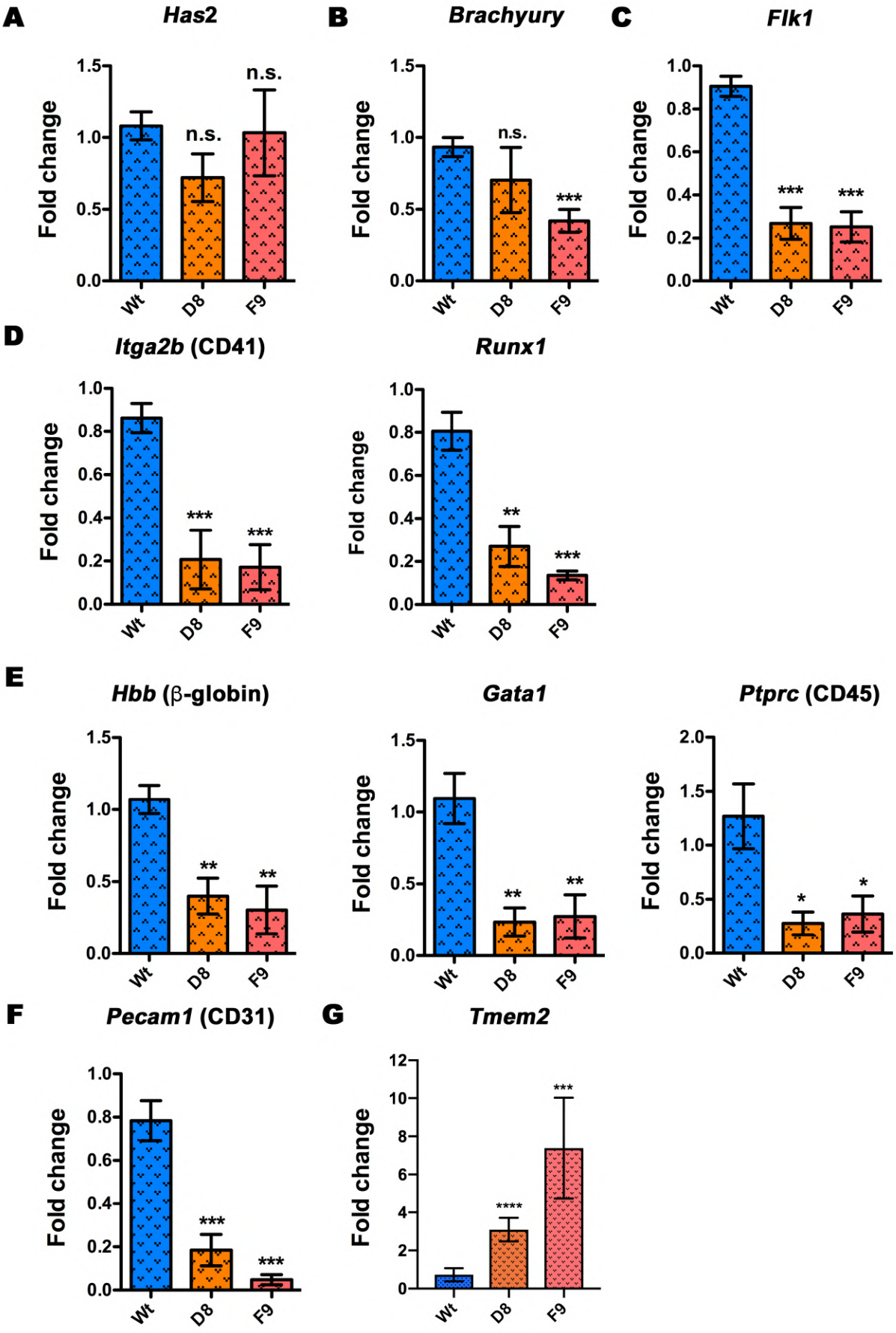

Supplemental Figure 8: Formation of vascular and blood lineages is impaired in *Vcan*-null embryoid bodies.
(A-F) 10-day differentiated embryoid bodies from three independent experiments were analyzed by RT-qPCR. *Has2* transcription in embryoid bodies was unaffected by the loss of versican. mRNA for the mesoderm marker *Brachyury* was significantly lower in F9 but not in D8 embryoid bodies contrasting with $Vcan^{hdf/hdf}$ embryos (main Fig. 3E). Expression of the hematovascular progenitor marker *Flk1,* blood lineage commitment progenitor markers *Itga2b* (CD41) and *Runx1*, differentiated blood markers *Hbb* (β-globin), *Gata1* and *Ptprc* (CD45) and endothelial marker *Pecam1* (CD31) was reduced in *Vcan*-null embryoid bodies (N=3 independent batches of 10 day embryoid bodies from each genotype, error bars= S.E.M., *, p<0.05; **, p<0.01; ***, p<0.0001).

Supplemental Figure 9

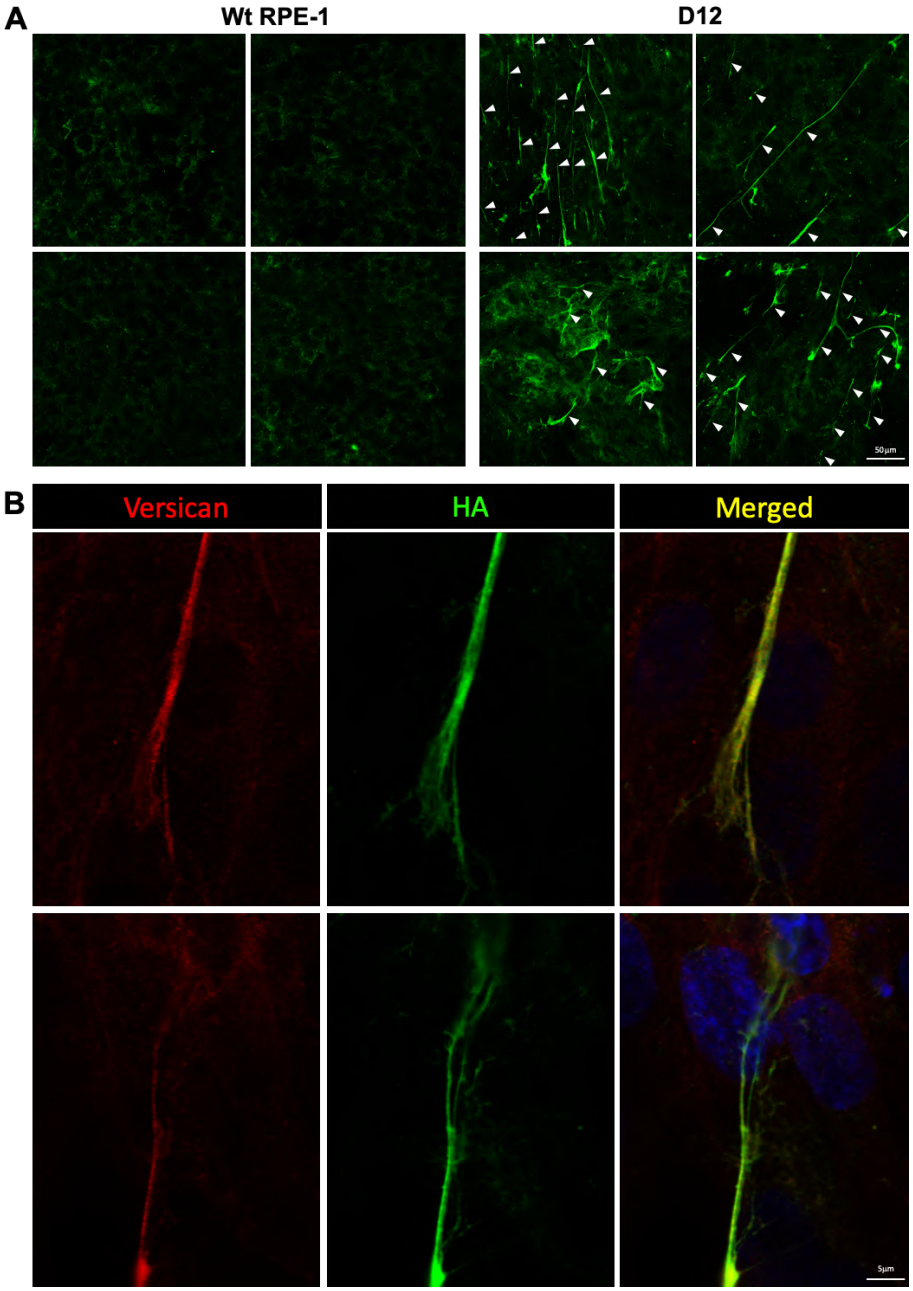

Supplemental Figure 9: Formation of hyaluronan and HA cables in *ADAMTS9* deficient RPE-1 cells in 25mM glucose
(A) Four independent representative areas of wild type RPE-1 and *ADAMTS9* deficient RPE-1 (D12) cell cultures stained with HAbp showing HA accumulation and numerous long HA-cables present in D12 cultures, but not parental RPE1 cells (white arrowheads).
(B) High-magnification confocal images showing two examples of long HA cables (green) decorated with versican (red). Scale bars = 50μm in **A** and 5μm in **B**.

Supplemental Figure 10

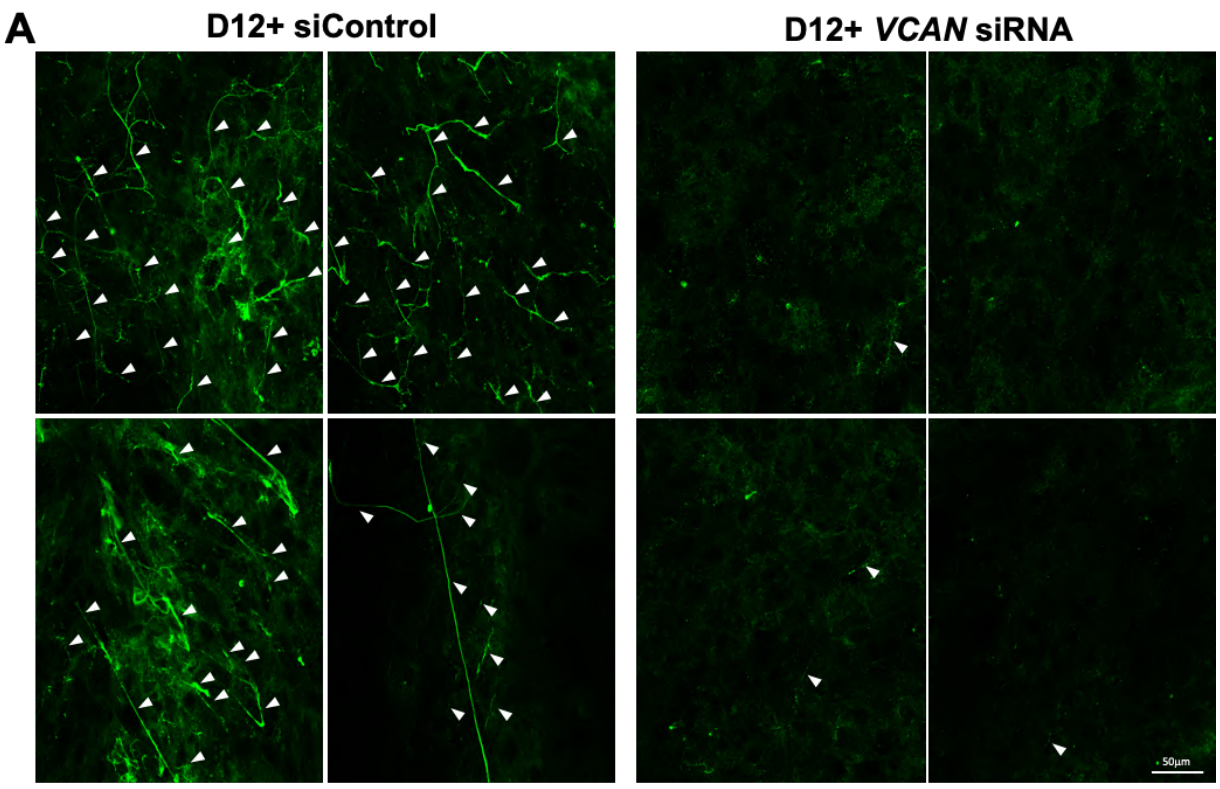

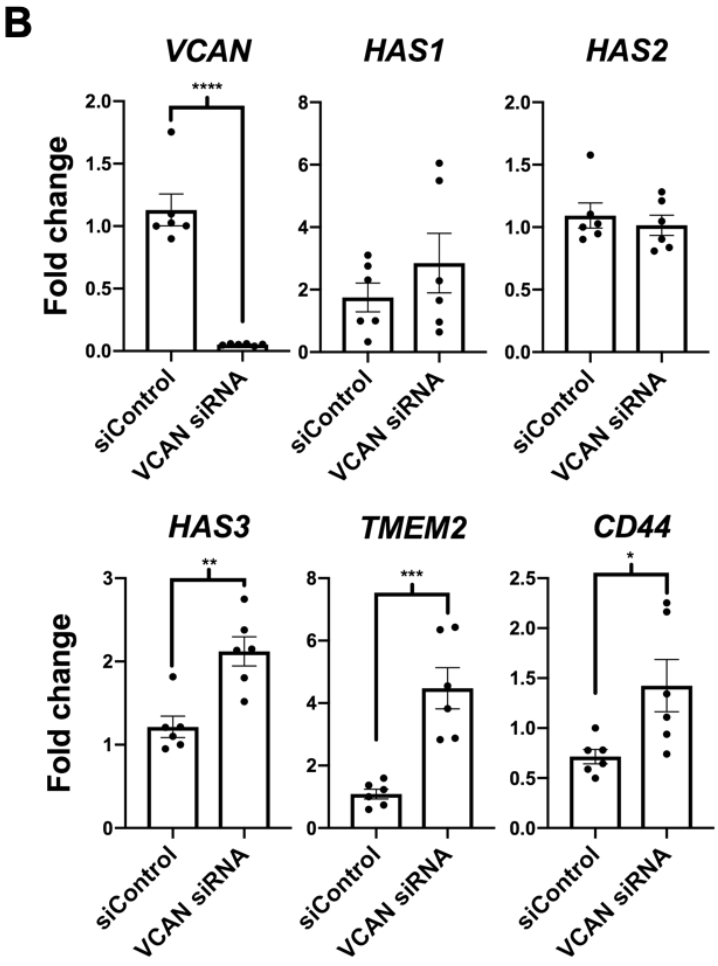

Supplemental Figure 10: Loss of HA and HA cables in *ADAMTS9*-deficient RPE-1 cells upon *VCAN* siRNA treatment

(A) Four independent representative areas of *ADAMTS9*-deficient RPE-1 (clone D12) cell cultures transfected with control siRNA (siControl) or *VCAN* siRNA, stained with HAbp showing loss of HA after *VCAN* knockdown, whereas HA-cables persist in siControl-treated D12 cells (white arrowheads).

(B) RT-qPCR of siControl and *VCAN* siRNA treated D12 cells showing decreased *VCAN* transcript levels upon siRNA treatment and upregulation of *HAS3, CD44* and *TMEM2* expression (n=3 independent siRNA treatment experiments, error bars= S.E.M., *, $p<0.05$; **, $p<0.01$; ***, $p<0.001$; ****, $p<0.0001$). Scale bar = 50µm in **A**.

Supplemental Figure 11

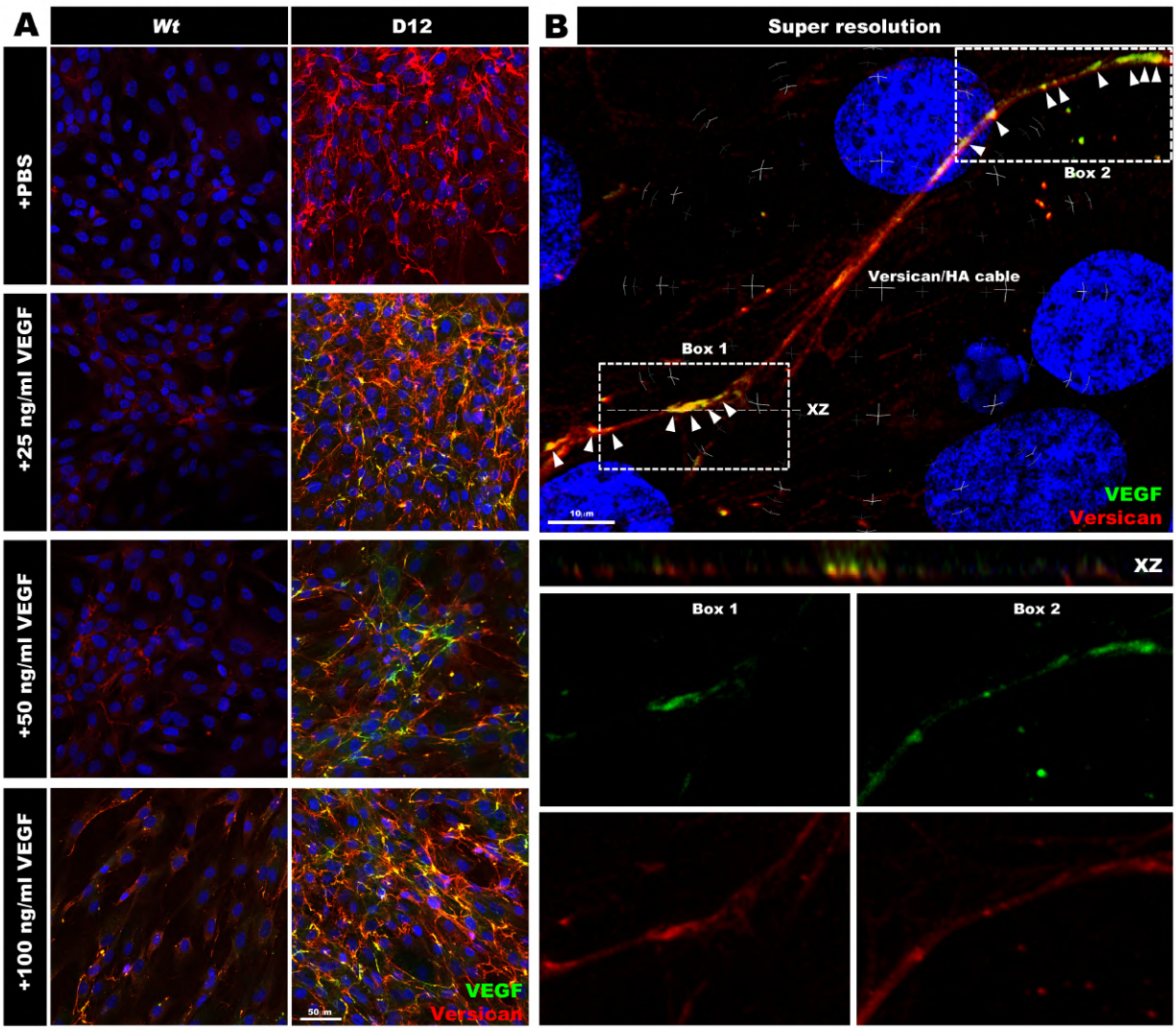

Supplemental Figure11: $VEGF_{165}$ co-localizes with versican in extracellular matrix of RPE-1 D12 cells in a dose-dependent manner
(A) Wild type RPE-1 and *ADAMTS9*-deficient RPE-1 (D12) cells treated with PBS or increasing concentrations of recombinant biotinylated $VEGF_{165}$ (green) showing dose-dependent VEGF staining intensity and colocalization with versican (red) in D12 cells. **(B)** Super-resolution confocal images of a long versican/HA cable showing patches of $VEGF_{165}$ (green) deposited along the versican stained cable (red). Nuclei are stained blue with DAPI. The upper merged panel shows some strongly co-staining regions (arrowheads), whereas the center panel shows co-staining in the X-Z plane. The lower panels show the single-color images of the areas marked as Box 1 and Box 2 in the upper panel. Scale bars = 50μm in **A** and 10μm in **B**.

Supplemental Figure 12

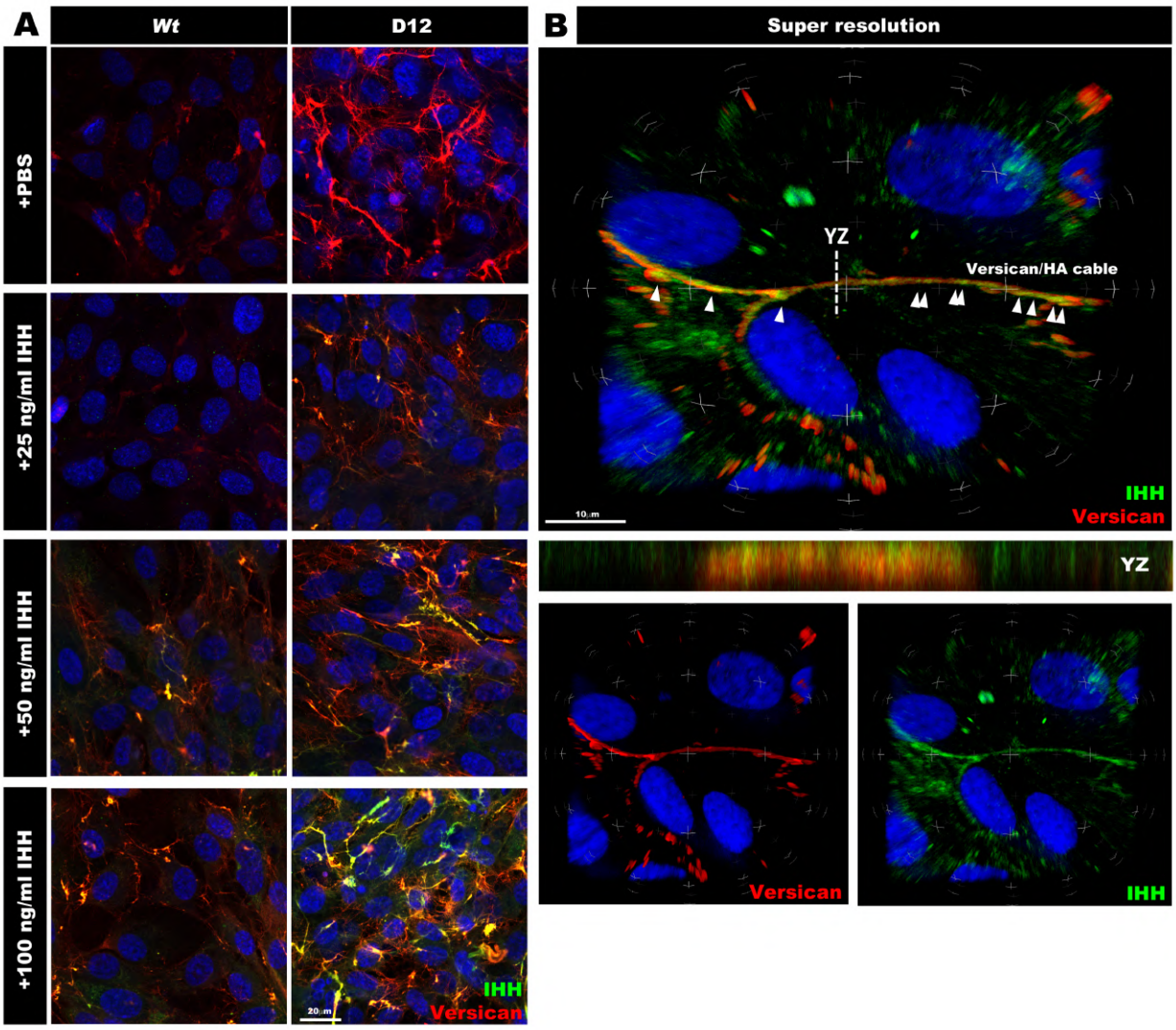

Supplemental Figure 12: Ihh co-localizes with versican in extracellular matrix in a dose-dependent manner.
(A) Wild type RPE-1 and *ADAMTS9* deficient (D12) cells treated with PBS or increasing concentrations of recombinant Ihh N-terminal domain (green) showing dose-dependent deposition and increased co-staining (yellow) with versican (red) in D12 cells. Nuclei are stained blue with DAPI.
(B) Super-resolution confocal image of a versican and HAbp-stained cable showing Ihh staining (green) along a versican stained cable (red). Strongly co-stained regions are indicated by arrowheads. The center panel shows the Y-Z plane. Bottom panels show single-color images of the area imaged in the upper panel. Scale bars = 20μm in **A** and 10μm in **B**.

Supplemental Table 1: Oligonucleotide primers used for RT-qPCR.

18S-F	5'-TTGACGGAAGGGCACCACCAG-3'
18S-R	5'-GCACCACCACCCACGGAATCG-3'
Actb-F	5'-GTGGGCCGCTCTAAGGCACCA-3'
Actb-R	5'-TGGCCTTAGGGTGCAGGGGG-3'
Brachyury-F	5'-GCTCTAAGGAACCACCGGTCATC-3'
Brachyury-R	5'-ATGGGACTGCAGCATGGACAG-3'
Myc-F	5'-TGACCTAACTCGAGGAGGAGCTGGAATC-3'
Myc-R	5'-AAGTTTGAGGCAGTTAAAATTATGGCTGAAGC-3'
Fn1-F	5'- GTCTAGGCGAAGGCAATGG-3'
Fn1-R	5'- CCTATAGGATGTCCGGGTGT-3'
Flk1-F	5'-ACTGCAGTGATTGCCATGTTCT-3'
Flk1-R	5'-TCATTGGCCCGCTTAACG-3'
Gata1-F	5'-AGCCTATTCTTCCCCCAAGTTTC-3'
Gata1-R	5'-CTCCACAGTTCACACACTCTCTGG-3'
Has2-F	5'-GGTCCAAGTGCCTTACTGAAAC-3'
Has2-R	5'-TGTAGAGCCACTCTCGGAAGTA-3'
Hbb-F	5'-GCTCTTGCCTGTGAACAATG-3'
Hbb-R	5'-GTCAGAAGACAGATTTTCAAATG-3'
Itga2b-F	5'-GAACCTGGAAGAAGCTGGCG-3'
Itga2b-R	5'-CTCCACTGTGGCTTCAGCTTG-3'
Nanog-F	5'-GGTTGAAGACTAGCAATGGTCTGA-3'
Nanog-R	5'-TGCAATGGATGCTGGGATACTC-3'
Oct4-F	5'-TCAGGTTGGACTGGGCCTAGT-3'
Oct4-R	5'-GGAGGTTCCCTCTGAGTTGCTT-3'
Pecam1-F	5'-CTGCCAGTCCGAAAATGGAAC-3'
Pecam1-R	5'-CTTCATCCACCGGGGCTATC-3'
Ptprc-F	5'-GAACATGCTGCCAATGGTTCT-3'
Ptprc-R	5'-TGTCCCACATGACTCCTTTCC-3'
Runx1-F	5'-GACCATCACCGTCTTTACAAATC-3'
Runx1-R	5'-TTGGTCTGATCATCTAGTTTCTGC-3'
Sox2-F	5'-GCACATGAACGGCTGGAGCAACG-3'
Sox2-R	5'-TGCTGCGAGTAGGACATGCTGTAGG-3'
Tmem2-F	5'-TCCTGGAGAAGCCAGAACTCAC-3'
Tmem2-R	5'-AGATGCACTGGCGTTGGTCGTT-3'
GAPDH-F	5'-AGCCTCAAGATCATCAGCAATG-3'
GAPDH-R	5'-CTTCCACGATACCAAAGTTGTCAT-3'
CD44-F	5'-CCAGAAGGAACAGTGGTTTGGC-3'
CD44-R	5'-ACTGTCCTCTGGGCTTGGTGTT-3'

HAS1-F	5'-CTGCGATACTGGGTAGCCTTCA-3'
HAS1-R	5'-CCAGGAACTTCTGGTTGTACCAG-3'
HAS2-F	5'-CCGATAACAGAAAATCTCTTTTTC-3'
HAS2-R	5'-AGCAGCCCATTGAACCAGAGAC-3'
HAS3-F	5'-AGCACCTTCTCGTGCATCATGC-3'
HAS3-R	5'-TCCTCCAGGACTCGAAGCATCT-3'
TMEM2-F	5'-ACCGAGCACATTCCAACTACCG-3'
TMEM2-R	5'-GGCAGAGATGATTGAGAGGAACG-3'

SUPPLEMENTAL METHODS

Mouse genotyping

Vcan$^{Tg(Hoxa1)1Chm}$ (*Vcan*^{hdf}) genotyping is described in Supplemental Figure 1. *Has2*^{flox} genotyping was carried out using the following primers; forward primer: 5' -TGCAGAATTTAGGGGCGAATTGGGAGCTAA-3', reverse primer: 5'-ATGAGGTTAGAGATTAGCAAGACTGAGTTC-3' which results in a 441 bp band for wild type and a 550 bp band for the floxed allele. *Sox2*Cre mice were genotyped using the following three-primer combination, primer-1: 5'-CTTGTGTAGAGTGATGGCTTGA-3', primer-2: 5'-TAGTGCCCCATTTTTGAAGG-3', primer-3: 5'-CCAGTGCAGTGAAGCAAATC-3' which results in a 207 bp band for wild type and a 165 bp band for *Sox2*Cre. The *Has2* null allele was genotyped using forward primer: 5'-CTTGAACCTTGAGTGTGCCATTTTGTAGTC-3' and reverse primer: 5'-CATTCTTGTTTTGAAGTTTGTTTCCTTGAC-3' which results in a 346 bp band.

Immunostaining and fluorescence microscopy

Immunostaining of E9.5 and E8.5 yolk sac was carried out on 30μm thick vibratome sections [1] or paraffin-embedded 7 μm sections. Immunostaining of cultured RPE-1 cells were carried out in 8-chamber cell culture slides (Fisher Scientific, catalog no. 354118). Immunostaining of collagen-embedded embryoid bodies were carried out in 4-chamber cell culture slides (Fisher Scientific, catalog no. 354114). Confocal microscopy images of whole mount mouse embryos and sections were acquired using a Leica TCS SP5 II multiphoton confocal microscope equipped with a 25X water immersion objective (Leica Microsystems, Wetzlar, Germany). For 3D-projection of whole mount Z-stacks, the Volocity 3D imaging software was used (version 6.3, PerkinElmer, Inc., Waltham, MA) in maximum intensity projection method. Confocal and super resolution microscopy of RPE-1 cells were carried out using a Leica TCS SP8 confocal microscopy equipped with Huygens deconvolution (HyVolution) capability as previously described [2] .

Methylcellulose colony formation assay

Single cell suspensions of E8.5 embryos, yolk sacs or day-10 embryoid bodies (EBs) were generated by incubation with trypsin for 10 minutes followed by disaggregation by pipetting with a 200 μL pipette tip until complete. 50,000 cells from each experimental group were transferred to a single 35 mm culture dish containing 1 mL of MethoCult GF M3534 culture medium (Methylcellulose medium with recombinant cytokines for mouse cells, Stem Cell Technologies, Vancouver, CA, catalog no. 03534) using a 3 mL syringe and 16-gauge needle, following the manufacturer's protocol. Triplicate cultures from each genotype were incubated for 14 days in a humidified, 5% CO_2, 37°C cell culture incubator. Blood colonies were counted using an inverted microscope. Aggregates with >50 cells were considered a colony-forming unit (CFU).

Primary antibodies and dilutions

For staining whole mount embryos, yolk sacs, vibratome sections and cell culture chamber slides the following antibodies, staining reagents and dilutions were used: Rabbit polyclonal anti-mouse versican GAGβ domain (Millipore-Sigma, catalog no. AB1033) 1:200; Rabbit polyclonal anti-versican cleavage site (anti-Vc) [3] 1:400; Rabbit polyclonal anti- versican V_0/V_1 neo cleavage antibody (DPEAAE) (Thermo Fisher, catalog no. PA1-1748A) 1:400; biotinylated hyaluronan binding protein (HAbp) (Millipore-Sigma, Calbiochem, catalog no. 385911) 1:100; rabbit polyclonal anti-fibronectin (Abcam, catalog no. Ab2413) 1:200; rabbit polyclonal anti-collagen-IV (Rockland antibodies and assays, catalog no. 600-401-106) 1:400; rat monoclonal anti-mouse Flk1 (clone Avas12, Thermo Fisher, catalog no. 17-5821-81) 1:200; hamster anti-mouse CD31 (Milipore-Sigma, catalog no. MAB1398Z) 1:400; FITC-conjugated anti-mouse CD41 (Biolegend, catalog no.133904) 1:100; mouse monoclonal Cy3 conjugated smooth muscle α-actin (Sigma-Aldrich, catalog no. C6198) 1:600; Alexa Fluor-568 phalloidin (Life Technologies, catalog no. A12380) 1:500; Streptavidin-FITC (Invitrogen, catalog no. SA1001) 1:400; Goat anti-mouse Ihh N-terminus (R&D Systems, catalog no. AF1705) 1:400; Mouse anti-Hapln1 (Link protein) (DSHB, 9/30/8-A-4-C) 1:100. All primary antibodies were diluted in 5% normal goat serum in PBST (PBS+ 0.1% Tween 20) and incubated overnight at 4°C. Alexa488, 568 or 647-conjugated secondary

antibodies against the corresponding species, or streptavidin conjugated Alexa488 or 568-labeled antibodies for HAbp detection were purchased from Invitrogen and were used at 1:400 dilution at room temperature for 2-3hrs. Slides were photographed using an Olympus BX51 upright microscope (Olympus, Center Valley, PA) connected to a Leica DFC7000T camera and Leica Application Suite v4.6 imaging software (both from Leica, Wetzlar, Germany).

Real time quantitative PCR (RT-qPCR) analysis

RNA from whole embryos, dissected yolk sacs, cultured cells or EBs was extracted using TRIzol reagent (ThermoFisher Scientific, catalog no. 15596026) according to manufacturer recommendations. 2 μg of RNA from each sample (embryo, yolk sac or EB pool) was used for cDNA synthesis using the high-capacity cDNA synthesis kit (Applied Biosystems, Thermo Fisher Scientific, catalog no. 4368814). RT-qPCR was carried out using a CFX96 Touch Real-Time PCR detection system (Bio-Rad Laboratories) with the Bullseye EvaGreen qPCR mix (MIDSCI, catalog no. BEQPCR-S), using primer pairs listed in the Supplemental Table-1. Each RT-qPCR sample was run in duplicate and 18s ribosomal RNA or *Actb* RNA were used for normalization of mouse genes while *GAPDH* was used for normalizing human gene expression and relative expression of genes was calculated by the ΔΔCt quantification method. An unpaired, two-tailed Student t-test was used to determine statistical significance using all RT-qPCR samples.

RNAscope *In-situ* hybridization and RNAseq database mining

4% PFA-fixed mouse embryos and yolk sacs were paraffin embedded and 7 μm thick sections were collected immediately prior to RNA in-situ hybridization. All RNAscope in situ probes and reagents were from Advanced Cell Diagnostics. The probes were: *Vcan* exon 7 (GAG-α) (catalog no. 428311), *Vcan* exon 8 (GAG-β) (catalog no. 428321), *Has2* (catalog no. 465171), *Flk1 (Kdr)* (catalog no. 414811) and *Runx1* (catalog no. 406671). In situ hybridization was carried out following the user manual for RNAScope 2.5 HD Red detection kit using the RNAscope HybEZ oven. Slides were photographed as described above.

A database containing recent analysis of 116,312 single cells (Pijuan-Sala B, et al., 2019) obtained from gastrulating mouse embryos spanning E6.5 to E8.5 was searched at specific gestational ages for expression of *Vcan, Kdr, Has2, Hapln1-4* and *Cd44*. Individual data panels were generated by the web portal for the deposited scRNAseq data accessed via: https://marionilab.cruk.cam.ac.uk/MouseGastrulation2018/

Western blotting

7.5% reducing SDS-PAGE was used for western blotting. Embryoid bodies were lysed in PBS containing 1% Tween 20 supplemented with a protease inhibitor cocktail (Roche, catalog no. 11873580001). Supernatants obtained after centrifugation at 1200 rpm for 10 minutes were treated with BSA-free *Proteus vulgaris* chondroitinase ABC (Sigma-Aldrich, catalog no. 3667) for 2 h at 37°C. Samples were boiled in Laemmli sample buffer (0.375% mM Tris.HCL, 9% SDS, 50% glycerol, 0.03% bromophenol blue, with 9% (v/v) β-mercaptoethanol) for 10 minutes followed by SDS-PAGE. Nitrocellulose membranes with transferred proteins were blocked in LI-COR Odyssey PBS blocking buffer (LI-COR Biosciences, Lincoln, NE catalog no. 927-40000) for 30 minutes in RT. Primary antibodies rabbit anti-mouse versican (GAGβ) antibody (1:1000) (Millipore-Sigma, catalog no. AB1033) or mouse monoclonal GAPDH antibody (1:5000) (Millipore-Sigma, catalog no. MAB374) were diluted in blocking buffer and incubated overnight at 4°C with gentle rocking. LI-COR IR dye secondary antibodies against mouse and rabbit antibodies (LI-COR Biosciences, Lincoln, NE) were used at 1:10000 dilutions in PBS to detect primary antibodies. A LI-COR Odyssey CLx scanner and the LI-COR Image Studio (ver. 4.0) was used to image western blots.

Fluorophore-assisted carbohydrate electrophoresis

FACE procedures used were essentially as previously published [4-6]. In brief, tissue was extensively digested with proteinase K and released glycosaminoglycans (GAGs) were isolated by ice-cold ethanol precipitation and centrifugation. GAGs were resuspended in 0.1 M ammonium

acetate, pH 7.0 and then digested overnight with *Streptomyces* hyaluronidase (200 mU) at 37° C for HA-FACE. HA digestion products were separated from other intact GAGs using ice-cold ethanol precipitation and centrifugation. The supernatant was then dried under vacuum centrifugation and reacted with 6.25 mM 2-aminoacridone (AMAC) and 625 mM sodium cyanoborohydride ($NaBH_3CN$) overnight at 37° C. The pellet was resuspended in 0.1 M ammonium acetate, pH 7.0 and then digested overnight with chondroitinase ABC (25 mU) at 37° C for CS-FACE. CS digestion products were separated from other intact GAGs using ice-cold ethanol precipitation and centrifugation. The supernatant was then dried under vacuum centrifugation and reacted with 6.25 mM AMAC and 625 mM $NaBH_3CN$ overnight at 37° C. AMAC-labeled HA and CS digestion products were loaded onto 20% (w/v) acrylamide gels and these products were resolved by electrophoresis at 500 V constant current over a 50-60 minute run time. FACE gels were imaged while still housed in the gel plates on a UVP ChemiDoc-It^2 515 system. Digital gel images were analyzed for AMAC-labeled HA and CS digestion product band intensities using ImageJ (NIH, Bethesda MD).

Transmission electron microscopy

E9.5 yolk sacs were harvested from timed pregnancies and fixed in 4% PFA + 2.5% glutaraldehyde in PBS overnight. Samples were dehydrated in an ethanol:PBS gradient and fully dehydrated samples were embedded in pure Eponate12 resin and allowed to polymerize overnight. Ultrathin sections (85 nm) were stained with uranyl acetate and lead citrate and viewed and imaged on a FEI Tecnai G2 Spirit BioTWIN Transmission Electron Microscope (FEI company, Hillsboro, OR) equipped with an Orius 832 CCD camera (Gatan, Inc., Pleasanton, CA).

Some E8.5 embryos were fixed in 4% PFA + 2.5% glutaraldehyde + 0.7% w/v ruthenium hexamine trichloride (Sigma-Aldrich, catalog no. 262005) in PBS overnight to optimize proteoglycan and cell membrane preservation [7] and embedded in Eponate 12 resin as described above. 1 micron-thick sections were stained with 1% toluidine blue containing 2% sodium borate for 30 seconds on a hot plate and washed with distilled water. Slides were mounted

with Cytoseal XYL mounting media (ThermoFisher Scientific, catalog no. 22-050-262) and imaged as described for routine microscopy.

$VEGF_{165}$ and Ihh treatment of RPE-1 cells

Wild type hTERT RPE-1 (ATCC, CRL-4000) cells and ADAMTS9 deficient RPE-1 cells [2] were cultured in 8-chamber cell culture slides (Fisher Scientific, catalog no. 354118) with a seeding density of 50,000 cells/chamber in DMEM F-12 culture medium containing 10% FBS for 48 hrs and washed with PBS and cultured in DMEM F-12 culture medium without FBS for an additional 24hrs in a cell culture incubator at 37C with 5% CO_2. Cells were cultured in DMEM F-12 medium containing 25, 50, 100 ng/ml recombinant human biotinylated $VEGF_{165}$ (R&D Systems, Cat. No. BT293-010) or recombinant human/mouse Ihh N-terminus (C2811) (R&D Systems, Cat. no. 1705-HH-025) for 6hrs. Cells were washed three times with PBS and fixed in 4% PFA. For versican depletion experiments, a previously validated highly potent *VCAN* siRNA (Ambion, Cat. no. S229335) [8-10], or control siRNA (Ambion, cat. no. 4390843) were added to the cell cultures 24 hrs after seeding using the Lipofectamine RNAiMAX protocol (Invitrogen, Cat. no. 13778) and cultured for 24 hrs prior to serum starvation and growth factor treatment. For treatment with chondroitinase ABC (0.2 U/ml in PBS, Sigma-Aldrich, Cat. no. C3667), cells were incubated overnight prior to the addition of recombinant $VEGF_{165}$ or Ihh. For co staining, recombinant $VEGF_{165}$ was detected using Streptavidin FITC (1:400, Invitrogen, SA1001), recombinant Ihh using anti mIhh-N antibody (1:400, R&D Systems, Cat. no. AF1705) and versican using the pVC antibody at a 1:400 dilution as previously described [2, 3]. Fixed cell culture chambers were blocked and incubated with primary antibodies in 5% normal goat serum for $VEGF_{165}$ experiments and 5% normal horse serum (Sigma-Aldrich, Cat. no. H0146-10ml) for Ihh experiments. Goat anti rabbit Alexa-568 secondary antibody (Invitrogen, Cat. no. A11011) and donkey anti goat Alexa-488 (Invitrogen, Cat. no. A11055) secondary antibodies were used at 1:600 dilution for detecting versican and Ihh primary antibodies. Super-resolution confocal microscopy was conducted as previously described [2].

Embryoid body formation and $VEGF_{165}$ induced angiogenic-sprouting

mESCs were cultured for two days till 100% confluent, gently washed with PBS and incubated with IMDM without LIF for an additional 48 h. IMDM without LIF was used in subsequent manipulations to form EBs. The medium was removed and 250 μl of trypsin was added to each plate and aspirated after a 30 second incubation, leaving a thin film of trypsin. Upon detachment and rounding of cells, 1 mL of IMDM was added to each plate, and a small pipette tip was used to generate small aggregates mechanically from the mESC sheet. The aggregates were transferred to 60 mm (non-adhesive) bacteriological dishes (Corning, catalog no. 351007) containing 5 mL of IMDM, where most curled and formed free-floating spheroids after 24 hrs. These 1-day EBs were transferred to a fresh bacteriological dish with 5 mL of IMDM and cultured for an additional 3 days. Ten to twenty 4-day old EBs from each genotype were transferred to a 4-well chamber (Fisher Scientific, catalog no. 354114) and embedded in bovine type 1 collagen (Corning, catalog no. 354231) containing 30 ng/mL recombinant $VEGF_{165}$ (PreproTech, catalog no. 100-20). 500 μL IMDM containing 30 ng/mL recombinant $VEGF_{165}$, was added atop each collagen gel and replaced very 4 days for a further 12 days. The collagen-embedded EBs were washed with PBS and fixed in 4% PFA for 15 min, permeabilized by three washes in PBS containing 0.3% Tween 20 for 30 minutes prior to immunostaining with anti-CD31 or anti-smooth muscle α-actin (SMA). For RT-qPCR, EBs in floating culture were incubated for 10 days (day-10 EBs). 300 μL of TRIzol reagent (ThermoFisher scientific, catalog no. 15596026) was used to harvest total RNA from each 60 mm plate.

Embryoid body vascular sprout quantifications

For quantifying EB vascular sprouts, collagen-embedded, fixed embryoid bodies in 4-chamber slides were imaged using an inverted bright field microscope. Images were analyzed by Image J-FIJI (NIH, Bethesda, MD), and the freehand drawing tool was used to trace the length of individual vascular sprouts. A total N= 72 wild type, 68 D8 and 68 F9 EBs were analyzed in 3

independent experiments. Lengths of 402 sprouts from wild type, 91 from D8 and 97 from F9 EBs were measured.

KEY RESOURCES TABLE

REAGENT or RESOURCE	SOURCE	IDENTIFIER
Primary antibodies		
Hamster monoclonal anti-mouse CD31	Millipore-Sigma	MAB1398Z
Rabbit polyclonal anti-versican	Millipore-Sigma	AB1033
Rabbit polyclonal anti-versican (pVC)	Apte Laboratory	N/A
Rabbit polyclonal anti-versican V_0/V_1 Neo cleavage (DPEAAE) antibody	Thermo Fisher	PA1-1748A
Rabbit polyclonal anti-fibronectin	Abcam	Ab2413
Rabbit polyclonal anti-collagen-IV	Rockland antibodies and assays	600-401-106
Rat monoclonal anti-mouse Flk1 (clone Avas12)	Thermo Fisher	17-5821-81
Rat monoclonal anti-mouse CD41	Biolegend	133904
Mouse monoclonal anti-smooth muscle α-actin	Sigma-Aldrich	C6198
Mouse monoclonal anti-GAPDH	Millipore-Sigma	MAB374
Goat anti-moue IHH N-terminus antibody	R&D Systems	AF1705
Mouse monoclonal anti-HAPLN1 (Link protein)	DSHB	9/30/8-A-4-C
Bacterial and Virus Strains		
One shot TOP10 chemically competent *E. coli* cells	Thermo Fisher	K280020
Biological Samples		
N/A	N/A	N/A
Chemicals, Peptides, and Recombinant Proteins		
Leukemia inhibitory factor (LIF)	EMD-Millipore	ESG1106
Recombinant $VEGF_{165}$	PreproTech	100-20
Recombinant biotinylated $VEGF_{165}$	R&D Systems	BT293-010
Recombinant human/mouse Ihh N-terminus	R&D Systems	1705-HH-025
Bovine type 1 collagen	Corning	354231
Proteus vulgaris chondroitinase ABC	Sigma-Aldrich	3667
Biotinylated hyaluronan binding protein (HAbp)	Millipore-Sigma, Calbiochem	385911
Alexa Fluor-568 phalloidin	Invitrogen	A12380
Streptavidin-FITC	Invitrogen	SA1001
Ruthenium hexamine trichloride	Sigma-Aldrich	262005
Protease inhibitor cocktail	Roche	11873580001
Critical Commercial Assays		
RNAscope mouse *Vcan* exon 7 (GAG-α) probe	Advanced Cell Diagnostics	428311
RNAscope mouse *Vcan* exon 8 (GAG-β) probe	Advanced Cell Diagnostics	428321
RNAscope mouse *Has2* probe	Advanced Cell Diagnostics	465171
RNAscope mouse *Kdr* (Flk1*)* probe	Advanced Cell Diagnostics	414811

RNAscope mouse *Runx1* probe	Advanced Cell Diagnostics	406671
MethoCult GF M3434	Stem Cell Technologies	03434
Bullseye EvaGreen qPCR mix	MIDSCI	BEQPCR-S
Deposited Data		
N/A	N/A	N/A
Experimental Models: Cell Lines		
R1 mouse embryonic stem cells (mESC)	CWRU Transgenic & Targeting Facility	[11] ATCC, SCRC-1011
Experimental Models: Organisms/Strains		
Mouse: *Vcan*$^{Hdf/+}$: Vcan$^{Tg(Hoxa1)1Chm}$/C57BL/6J	N/A	MGI:1857689 [12]
Mouse: *Has1*$^{-/-}$*; Has3*$^{-/-}$ double knockout	N/A	[13]
Mouse: *Has2* $^{tm1.1Yama}$ allele	N/A	MGI:4360705 [14]
Mouse: *Sox2Cre*^{tg}	N/A	JAX:008454 [15]
Oligonucleotides		
See Supplemental Table 1 for RT-qPCR primers	This paper	N/A
VCAN siRNA	Ambion	S229335
Control siRNA	Ambion	4390843
Recombinant DNA		
mVcan-E2-U6gRNA-Cas9-2A-GFP	Sigma-Aldrich	target ID MM0000080027
mVcan-E3-U6gRNA-Cas9-2A-GFP	Sigma-Aldrich	target ID MM0000080028
pCR-Blunt II-TOPO	Life Technologies	K2800-40
Software and Algorithms		
LI-COR Image Studio (ver. 4.0)	LI-COR	N/A
Volocity 3D imaging software (ver. 6.3)	PerkinElmer	N/A
Image J	NIH	https://imagej.nih.gov/ij/
Other		
N/A		

Supplemental References

1. Nandadasa, S., C.M. Nelson, and S.S. Apte, *ADAMTS9-Mediated Extracellular Matrix Dynamics Regulates Umbilical Cord Vascular Smooth Muscle Differentiation and Rotation.* Cell Rep, 2015. **11**(10): p. 1519-28.
2. Nandadasa, S., et al., *Secreted metalloproteases ADAMTS9 and ADAMTS20 have a non-canonical role in ciliary vesicle growth during ciliogenesis.* Nat Commun, 2019. **10**(1): p. 953.
3. Foulcer, S.J., et al., *Determinants of versican-V1 proteoglycan processing by the metalloproteinase ADAMTS5.* J Biol Chem, 2014. **289**(40): p. 27859-73.
4. Calabro, A., et al., *Microanalysis of enzyme digests of hyaluronan and chondroitin/dermatan sulfate by fluorophore-assisted carbohydrate electrophoresis (FACE).* Glycobiology, 2000. **10**(3): p. 273-81.
5. Calabro, A., V.C. Hascall, and R.J. Midura, *Adaptation of FACE methodology for microanalysis of total hyaluronan and chondroitin sulfate composition from cartilage.* Glycobiology, 2000. **10**(3): p. 283-93.
6. Midura, R.J., et al., *Quantification of hyaluronan (HA) using a simplified fluorophore-assisted carbohydrate electrophoresis (FACE) procedure.* Methods Cell Biol, 2018. **143**: p. 297-316.
7. Hunziker, E.B., W. Herrmann, and R.K. Schenk, *Ruthenium hexammine trichloride (RHT)-mediated interaction between plasmalemmal components and pericellular matrix proteoglycans is responsible for the preservation of chondrocytic plasma membranes in situ during cartilage fixation.* J Histochem Cytochem, 1983. **31**(6): p. 717-27.
8. Francis-West, P., et al., *Signalling interactions during facial development.* Mech Dev, 1998. **75**(1-2): p. 3-28.
9. Gueye, N.A., et al., *Versican Proteolysis by ADAMTS Proteases and Its Influence on Sex Steroid Receptor Expression in Uterine Leiomyoma.* J Clin Endocrinol Metab, 2017. **102**(5): p. 1631-1641.
10. Keire, P.A., et al., *Inhibition of versican expression by siRNA facilitates tropoelastin synthesis and elastic fiber formation by human SK-LMS-1 leiomyosarcoma smooth muscle cells in vitro and in vivo.* Matrix Biol, 2016. **50**: p. 67-81.
11. Nagy, A., et al., *Derivation of completely cell culture-derived mice from early-passage embryonic stem cells.* Proc Natl Acad Sci U S A, 1993. **90**(18): p. 8424-8.
12. Yamamura, H., et al., *A heart segmental defect in the anterior-posterior axis of a transgenic mutant mouse.* Dev Biol, 1997. **186**(1): p. 58-72.
13. Arranz, A.M., et al., *Hyaluronan deficiency due to Has3 knock-out causes altered neuronal activity and seizures via reduction in brain extracellular space.* J Neurosci, 2014. **34**(18): p. 6164-76.
14. Matsumoto, K., et al., *Conditional inactivation of Has2 reveals a crucial role for hyaluronan in skeletal growth, patterning, chondrocyte maturation and joint formation in the developing limb.* Development, 2009. **136**(16): p. 2825-35.
15. Hayashi, S., et al., *Efficient gene modulation in mouse epiblast using a Sox2Cre transgenic mouse strain.* Mech Dev, 2002. **119 Suppl 1**: p. S97-S101.